Maintenance of mitochondrial integrity in midbrain dopaminergic neurons governed by a conserved developmental transcription factor

Federico Miozzo[1], Luca Stickely[1], Damla Tas[1,2], Nicolas Loncle[1,3], Irina Nikonenko[4], Michaela Dorcikova[1], Eva P. Valencia-Alarcón[1], Peter Bou Dib[5,6] and Emi Nagoshi[1,*]

[1]Department of Genetics and Evolution and Institute of Genetics and Genomics of Geneva (iGE3), University of Geneva, CH-1211, Geneva 4, Switzerland

[2]Present address: The Janssen Pharmaceutical Companies of Johnson & Johnson, Bern, Switzerland

[3]Present address: Puma Biotechnology, Inc., Berkeley, California

[4]Department of Basic Neurosciences and the Center for Neuroscience, CMU, University of Geneva, CH-1211, Geneva 4, Switzerland

[5]Institute of Cell Biology, University of Bern, CH-3012, Bern, Switzerland

[6]Present address: Department of Chemistry, Humboldt-Universität zu Berlin, 12489 Berlin, Germany

[*]Corresponding author: Emi.Nagoshi@unige.ch

ABSTRACT

The degeneration of dopaminergic (DA) neurons in the substantia nigra is a hallmark of Parkinson's Disease (PD). Dysregulation of developmental transcription factors is implicated in dopaminergic neurodegeneration, but the underlying molecular mechanisms remain largely unknown. *Drosophila Fer2* is a prime example of a developmental transcription factor required for the birth and maintenance of midbrain DA neurons. Using an approach combining ChIP-seq, RNA-seq, and genetic epistasis experiments with PD-linked genes, here we demonstrate that *Fer2* controls a transcriptional network to maintain mitochondrial structure and function, and thus confers dopaminergic neuroprotection against genetic and oxidative insults. We further show that conditional ablation of *Nato3,* a mouse homolog of *Fer2*, in differentiated DA neurons results in locomotor impairments and mitochondrial abnormality in aged mice. Our results reveal the essential and conserved role of *Fer*2 homologs in the mitochondrial maintenance of midbrain DA neurons, opening new perspectives for modelling and treating PD.

INTRODUCTION

Midbrain dopaminergic (mDA) neurons play a central role in controlling key brain functions, including voluntary movement, associative learning, motivation and cognition[1]. The progressive and selective degeneration of mDA neurons in the substantia nigra (SN) results in a loss of nigrostriatal DA neurotransmission, leading to the motor symptoms of Parkinson's disease (PD). Although PD was first described over 200 years ago and is the most prevalent neurodegenerative movement disorder, the exact pathologic mechanisms underlying this disease remain unclear. Treatment options are limited to symptomatic relief with DA replacement therapy[2,3]. Thus, the identification of targets for disease-modifying therapies that reverse or hinder neurodegeneration in PD is greatly needed.

PD is a multifactorial disorder caused by a combination of genetic and environmental factors[4]. Increasing evidence indicates that PD risk factors lead to common pathological processes, including excessive production of reactive oxygen species (ROS), axonal pathology, neuroinflammation, defects in the ubiquitin-proteasome system, and mitochondrial dysfunction[5,2]. In particular, mitochondrial impairment is integral to most other pathological cellular processes and thought to play a central role in dopaminergic neurodegeneration. Complex I activity is reduced in the brains of PD patients, and mitochondrial toxins such as 1-methyl-4-phenyl-1,2,3,6-tetrahydropyridine (MPTP) and rotenone potently induce SN degeneration. The findings that multiple genes linked to familial PD, such as *PINK1*, *Parkin*, *LRRK2*, *SNCA* and *DJ-1*, directly or indirectly affect mitochondrial physiology further support this notion[6,7].

Although several genes linked to rare monogenic forms of PD have been identified, genetic susceptibility factors for sporadic PD, which accounts for approximately 90% of cases, remain largely unknown. In this regard, it is noteworthy that dysregulation of transcription factors required for mDA development is implicated in PD. Numerous

transcription factors required for various aspects of mDA neurons development, including *En1*, *En2*, *Lmx1a*, *Lmx1b*, *Foxa1*, *Foxa2*, *Nurr1*, *Pitx3* and *Otx2*, remain expressed in the adult brain and are crucial for the survival and function of differentiated mDA neurons in mice[8–16]. Genome-wide association studies (GWAS) have shown that genetic variants of developmental transcription factors are highly represented in sporadic PD patients[17,18]. Moreover, overexpression of *Nurr1*, *Foxa2*, *En1* or *Otx2* prevents the loss of DA neurons in murine PD models[19–21]. Therefore, a better comprehension of the genetic networks controlled by developmental transcription factors in differentiated mDA neurons may advance our molecular understanding of neurodegeneration in PD and open new therapeutic options.

Drosophila offers a powerful model system to investigate molecular mechanisms of PD pathogenesis *in vivo*, due to the abundance of genetic tools, the conservation of most PD-related pathways and familial PD-linked genes, and its relatively simple nervous system[22,23]. The adult fly midbrain contains approximately a dozen clusters of DA neurons projecting to different areas[24]. Although the anatomical arrangements of DA neurons in *Drosophila* and vertebrates differ considerably, recent works have highlighted the functional homology of some of the dopaminergic circuits[25]. The protocerebral anterior medial (PAM) cluster is the largest subgroup containing approximately 80% of all *Drosophila* brain DA neurons. PAM neurons are highly heterogeneous in their function and projection patterns, modulating various behavior including associative learning, sleep, and locomotion[26,27]. Remarkably, some of the PAM neurons are required for the startle-induced climbing, a locomotor behavior found to be defective in multiple PD models[27–29], rendering the PAM cluster partially analogous to the mammalian SN. Dopaminergic innervation from the PPL1 and PPM3 clusters to the central complex also appear to be functionally homologous to the nigrostriatal pathway and is reported to be impaired in some PD models[25,30,31].

The notion that developmental transcription factors play critical roles in the

maintenance of adult DA neurons is shared between flies and mammals, as supported by our recent studies of *Drosophila Fer2* gene. *Fer2* encodes a basic helix-loop-helix (bHLH) transcription factor required for the development of DA neurons in the PAM cluster, and fewer PAM neurons are formed in *Fer2*^{2} hypomorphic mutants. Additionally, *Fer2*^{2} mutant flies display a progressive loss of PAM neurons in adulthood, locomotor impairment that can be improved by L-DOPA administration, and increased ROS levels in the brain. PAM neurons deficient for *Fer2* accumulate abnormal mitochondria and show autophagy dysfunction. *Fer2* expression persists into adulthood in PAM neurons and increases in response to oxidative stress. Importantly, the maintenance of mitochondrial integrity and the survival of PAM neurons in aged flies require the presence of *Fer2* in PAM neurons in adulthood[28,29]. Taken together, these lines of evidence establish the dual role of *Fer2* in development and lifelong maintenance of DA neurons in the PAM cluster, and suggest that molecular studies of *Fer2* function will shed light on the mechanisms of dopaminergic neurodegeneration relevant to PD.

In the present study, we ask how *Fer2* maintains DA neurons throughout adulthood and whether its function is conserved in mammals. We address these questions by analyzing functional interaction between *Fer2* and familial PD-linked genes, by identifying *Fer2* target genes and by generating mice with a conditional deletion of *Nato3,* a murine homolog of *Fer2*, in differentiated DA neurons. This combined approach demonstrates that *Fer2* is a master regulator of a transcriptional network controlling mitochondrial integrity and function, and thereby confers dopaminergic neuroprotection in multiple genetic and toxin models of PD. *Nato3* is known to be required for the genesis of mDA neurons[32–34] but its post-developmental role has never been studied. We show here for the first time that selective ablation of *Nato3* in differentiated DA neurons leads to age-dependent motor impairment and a loss of mitochondrial integrity in mDA neurons. Taken together, our results indicate that

Fer2 and *Nato3* share an essential role in maintaining mitochondrial health and dopaminergic function, offering new opportunities to study the selective vulnerability of mDA neurons and to develop therapeutic interventions for PD.

RESULTS

Fer2 overexpression protects PAM dopaminergic neurons from genetic and oxidative insults

To explore the genetic mechanisms underlying the role of *Fer2* in the maintenance of DA neurons, we investigated whether *Fer2* loss or gain of function affects the survival of DA neurons in genetic models of PD. Mutations in the *leucine-rich repeat kinase 2* (*LRRK2*) gene are the most common cause of familial PD and also predispose carriers to sporadic PD[35]. Because pathogenic *LRRK2* variants are considered to be gain-of-function mutants, most fly models of *LRRK2*-linked PD employ overexpression of wild-type or mutant forms of *LRRK2* or its fly homolog. We thus overexpressed wild-type or mutant *Drosophila Lrrk* via the GAL4/UAS system using PAM neuron-specific drivers, *Fer2-GAL4* or *R58E02-GAL4*[26,28]. The number of surviving DA neurons was assessed by immunostaining with anti-tyrosine hydroxylase (TH) antibodies.

Forced expression of either wild-type or LRRK I1915T mutant, which is homologous to the human pathogenic LRRK2 I2020T variant[35,36], leads to a loss of PAM neurons. A neuronal loss of approximately 10% of was observed in 1-day-old flies, and thereafter the cell loss progressed in an age-dependent manner, indicating that *Lrrk* gain of function impairs both the development and the maintenance of PAM neurons (Supplementary Fig. 1a and Fig. 1a-b). Remarkably, overexpression of *Fer2* in PAM neurons prevented PAM neuron loss induced by *Lrrk* gain of function (Fig. 1a-b). Forced expression of *Lrrk* in $Fer2^{2}$ heterozygous background resulted in PAM neuron loss to a similar extent as in wild-type

background. *Lrrk* overexpression in *Fer2*^{2} homozygous mutants additively enhanced PAM neuron loss compared with either of the single genetic perturbations (Supplementary Fig. 1b). These results suggest that *Fer2* and *Lrrk* act in independent pathways but *Fer2* can attenuate *Lrrk*-induced neuronal damage.

Mutations in the *PRKN* gene, which encodes the E3 ubiquitin ligase Parkin, are linked to autosomal recessive juvenile PD[37]. *Drosophila parkin* loss-of-function mutant *park*^{1} exhibits PD-like phenotypes, including locomotor deficits, mitochondrial impairments and loss or shrinkage of a few subclasses of DA neurons[38,39]. We examined *park*^{1} mutant brains with anti-TH immunostaining and found that DA neuron loss occurs also in the PAM cluster (Fig. 1c). A greater loss of PAM neuron was observed in *park*^{1}, *Fer2*^{2} double mutants than in either of the single mutants. The increase in cell loss was additive but not synergistic, suggesting that *parkin* and *Fer2* do not act in the same linear pathway (Supplementary Fig. 1c). However, interestingly, the overexpression of *Fer2* in PAM neurons significantly reduced *park*^{1}-induced cell loss (Fig. 1d).

Parkin mutations lead to severe defects in mitochondrial morphology and function in all organisms studied thus far, including flies[40–43]. We therefore examined whether *Fer2* overexpression ameliorates mitochondrial morphology in DA neurons of *park*^{1} flies by expressing mitochondria-targeted GFP (mitoGFP) in PAM neurons. In contrast to the reticular mitochondria observed in control flies, the majority of mitochondria appeared to be more rounded in PAM neurons of *park*^{1} mutants (Fig. 1e). This observation was quantitatively confirmed by the analysis of mitochondria circularity, which showed a shift towards more globular mitochondria in *park*^{1} compared with control (*park*^{1}/+) flies (Fig. 1f). Remarkably, the overexpression of *Fer2* in PAM neurons restored tubular mitochondrial morphology in *park*^{1} flies (Fig. 1e-f).

The findings that *Fer2* overexpression cell-autonomously prevents PAM neuron loss

in two independent familial PD models and ameliorates mitochondrial morphology defects in *park*[1] mutants suggests that *Fer2* gain of function might confer dopaminergic neuroprotection against a broad spectrum of genetic and chemical insults. We therefore tested if *Fer2* overexpression can protect DA neurons from damage caused by oxidative stress, using an assay in which flies were exposed to a non-lethal dose of hydrogen peroxide (H_2O_2). 7-day-old flies were fed with 5% H_2O_2 for 24h, and 7 days later DA neurons in the brains were examined by anti-TH immunostaining. This treatment triggered the loss of approximately 10% of DA neurons in the PAM cluster in w^{1118} flies, $Fer2^2$/+ flies and flies carrying a PAM-specific driver. The PAM neuron loss was exacerbated in flies homozygous for the $Fer2^2$ allele, consistent with our previous finding that *Fer2* inactivation renders PAM neurons more vulnerable to oxidative stress[28,29]. In contrast, *Fer2* overexpression in PAM neurons prevented H_2O_2-induced PAM neuron loss (Fig. 2a). These results indicate that *Fer2* gain of function protects DA neurons in the PAM cluster from oxidative insults.

ROS production increases as flies age[44]. Interestingly, we found an age-dependent increase in FER2 protein levels in PAM neurons, parallel to the augmentation of ROS levels in the brain (Fig. 2b-e). Combined with the fact that *Fer2* loss of function causes a progressive loss of PAM neurons, this finding suggests that FER2 is upregulated to protect PAM neurons from age-dependent increases in endogenous oxidative stress. Taken together, these results provide evidence that *Fer2* is a potent neuroprotective transcription factor for PAM dopaminergic neurons, counteracting various genetic and oxidative insults.

Identification of *Fer2* direct targets by a combination of ChIP-seq and RNA-seq approaches

To investigate how *Fer2* elicits dopaminergic neuroprotection, we wished to identify *Fer2* transcriptional targets. To this end, we first determined the genome-wide binding sites of

FER2 using chromatin immunoprecipitation coupled to sequencing (ChIP-seq). Since FER2-specific antibodies were unattainable, ChIP-seq was performed on the heads of 14-day-old flies harboring a *Fer2::GFP::V5* genomic transgene in *Fer2*^{1} mutant background[28], using anti-V5 antibody (Fig. 3a). *Fer2::GFP::V5* is functional and recapitulates the physiological dosage and expression pattern of *Fer2*, as it rescues PAM neuron loss and locomotor defects in *Fer2*^{1} mutants (Supplementary Fig. 2b-c) and is expressed in PAM neurons but scarcely in other cells in the brain (Supplementary Fig. 2a), in agreement with existing single-cell RNA-seq data[45,46]. We identified 269 FER2-bound regions, which were annotated to 279 putative *Fer2* target genes (Supplementary Table 1). FER2-bound sequences were highly enriched with a 12-nucleotide motif containing a canonical bHLH binding site (CANNTG), validating the specificity of the procedure (Fig. 3b).

The biding of transcription factors to chromatin does not necessarily lead to transcriptional regulation of nearby genes. To determine which binding events regulate proximal gene expression, we next identified transcripts that are up- or downregulated after a transient overexpression of *Fer2* and compared these transcripts with the ChIP-seq data. The heat-inducible *hs-GAL4* was used to ubiquitously but acutely express *Fer2,* and RNA-seq was performed on fly heads collected 12 and 48 h after a 3-h heat shock treatment. The same heat-shock treatment was applied to the flies carrying *hs-GAL4* but not *UAS-Fer2* to identify and exclude from our analysis any heat-responsive gene (Fig. 3c). These experiments identified 328 genes (12 h after heat shock) and 916 genes (48 h after heat shock) differentially expressed in the head following *Fer2* overexpression (Fig. 3c and Supplementary Table 2). Then, by comparing the head RNA-seq and *Fer2* ChIP-seq data, we found 32 genes that were present in FER2 ChIP-seq and also differentially expressed 48 h after *Fer2* overexpression. These genes are considered as potential *Fer2* transcriptional targets. The overlap was statistically highly significant (hypergeometric probability = 0.0004).

In contrast, there was no statistically significant overlap between the ChIP-seq data and the genes differentially expressed 12 h after heat-shock, therefore we focused our subsequent analysis on the data set obtained at the 48 h timepoint. The ChIP-seq profiles and RNA-seq data of two *Fer2* targets, *CG8128* and *skd*, are presented as examples in Fig. 3d. Because *Fer2* expression is largely restricted to PAM neurons, the majority of FER2 ChIP signal represents FER2 binding within PAM neurons, whereas whole-head RNA-seq following *Fer2* induction detects genes also expressed outside the PAM cluster. Therefore, to determine whether the *Fer2* targets identified above are expressed in PAM neurons, we profiled the transcriptome of isolated PAM neurons. Indeed, the majority (26 out of 32) of *Fer2* target genes identified by the ChIP-seq/head RNA-seq intersectional analysis were found to be expressed in PAM neurons (Fig. 4a-b), validating this subset of 26 genes as *bona fide* direct transcriptional targets of *Fer2* (Fig. 4c, Supplementary Table 3).

A further analysis of the 26 *bona fide* targets revealed that *Fer2* preferentially binds to introns of the target genes and acts as a repressor in most instances, as the majority of direct targets are downregulated after acute *Fer2* overexpression (Fig. 4d-e). A large fraction of the 26 *Fer2* direct targets are involved in the regulation of gene expression, including transcription factors (*ftz-f1*, *Eip75B*, *Eip93F*, *Snoo*), transcriptional coregulators (*skd*), components of chromatin remodeling complexes (*Smr*, *osa*, *sba*) and histone modifiers (*gpp*). These genes show a significant interconnectivity (p-value = 0,00006) either physically or functionally, as inferred from STRING database analysis, suggesting that they may cooperate to regulate downstream gene expression (Fig. 4c).

Multiple *Fer2* direct target genes contribute to the maintenance of PAM dopaminergic neurons

Next, we assessed whether *Fer2* direct target genes have roles similar to *Fer2* by

manipulating their expression levels individually in PAM neurons and monitoring neuronal survival. To mimic the effect of *Fer2* loss of function, target genes upregulated by *Fer2* were knocked-down via RNAi, and genes downregulated by *Fer2* were overexpressed in PAM neurons. PAM neurons were examined at the age of 35 days with anti-TH staining. 19 out of 26 *Fer2* direct targets were tested in this assay, since transgenic lines for RNAi or overexpression for 7 genes were unavailable or lethal when combined with the *Fer2-GAL4* driver. The majority of the transgenic lines used in this assay have been validated in previous studies. Remarkably, genetic manipulation of one third of the tested genes (6 out of 19) caused a significant loss of PAM neurons compared with the driver-only control, thus partially recapitulating the phenotype of *Fer2* loss of function (Fig. 4f and Supplementary Table 3). These results broadly confirm that the ChIP-seq and RNA-seq intersectional analysis identified a panel of *Fer2* direct targets that contribute to the role of *Fer2* in the development and maintenance of PAM neurons.

Fer2 is a master regulator of mitochondrial health and function

Since many *Fer2* direct targets are transcriptional regulators, *Fer2* most likely orchestrates the expression of a larger set of secondary targets to promote the survival of PAM neurons. To decipher downstream biological processes controlled by *Fer2*, we profiled the transcriptome of isolated PAM neurons following constitutive, PAM-specific *Fer2* overexpression (Fig. 4a). We reasoned that this approach should capture the long-term consequences of *Fer2* overexpression on gene expression in PAM neurons. A comparison of PAM neuron transcriptomes of flies overexpressing *Fer2* and age-matched controls identified 132 differentially expressed genes (DEGs) (24 genes upregulated and 108 genes downregulated; $p<0.01$). These genes were distinct from the 26 direct targets and were considered as *Fer2* secondary targets (Fig. 4a-b; Supplementary Table 4).

Gene ontology (GO) analysis of *Fer2* secondary targets revealed a marked enrichment of nuclear-encoded mitochondrial genes, particularly among up-regulated genes. These include a component of the electron transport chain (ETC) (*ND-15*), genes involved in the assembly or maturation of ETC complexes (*Sdhaf3*, *CG7639*, *Cchl*, *CG5037*), and the mitochondrial *Superoxide dismutase 2* (*Sod2*) (Fig. 4g and Supplementary Table 4.). As a crucial player in the cellular antioxidant response, SOD2 is localized to the mitochondrial matrix and catalyzes superoxide ($O_2\bullet^-$) to the less reactive H_2O_2[47]. Remarkably, *Sod2* overexpression in PAM neurons partially but significantly prevented neuronal loss in *Fer2*[2] mutant flies, which suggests that *Sod2* acts downstream of *Fer2* to contribute to dopaminergic neuroprotection (Fig. 4h). Combined with the finding that *Fer2* regulates the expression of numerous mitochondrial genes, these results demonstrate that *Fer2* plays a prominent role in the maintenance of mitochondria.

To explore how *Fer2* direct targets control a large set of secondary targets, we searched for transcription factor binding sites that are significantly overrepresented in the promoters of DEGs in PAM RNA-seq. Seven binding motifs were found to be enriched, including those for Broad, Dichate and USP, which are expressed in PAM neurons. Interestingly, these genes are known to form complexes or functionally interact with FTZ-F1, a *Fer2* direct target[48,49] (STRING database). Therefore, gene regulatory networks initiated by *Fer2* may be mediated by FTZ-F1 together with these factors (Supplementary Fig. 3a-b). Our finding that *ftz-f1* is necessary for PAM neuron maintenance (Fig. 4f) supports this prediction. Another *Fer2* direct target, SMRTR, can interact with USP[50], and may thus initiate a second pathway to control gene networks in PAM neurons (Supplementary Fig. 3a-b).

Conditional deletion of *Nato3* in differentiated DA neurons leads to locomotor deficits in aged mice

Since *Fer2* is required for the maintenance of mitochondrial health and integrity in DA neurons, we wondered whether the mammalian homolog of *Fer2* has a similar role. Blast searches found four mammalian bHLH transcription factors with a significant similarity to FER2, namely P48/PTF1A, NATO3 (N-TWIST, FERD3L), TCF15, and TWIST1. Interestingly, it has been shown that *Nato3* is expressed in the progenitors of mDA neurons and is required for dopaminergic neurogenesis, analogously to the role of *Fer2* in the genesis of DA neurons in flies[32,33,51]. Furthermore, RNA-seq data from the Genotype-Tissue Expression (GTEx) project (the GTEx Consortium, Nat Genetics, 2013) indicate that, among human tissues, *Nato3* expression is relatively restricted to the SN of the adult brain (Fig. 5a). Based upon these evident similarities in the protein sequence, the expression in mDA neurons and the role in the development of mDA neurons, we consider *Nato3* to be a functional homolog of *Fer2*.

To investigate whether *Nato3* is involved in the maintenance of postnatal mDA neurons, we first determined its expression levels and specificity in the mouse brain. Reverse Transcription quantitative PCR (RT-qPCR) analysis of dissected brain regions displayed a significant enrichment of *Nato3* transcripts in the midbrain of 4-month-old mice (Fig. 5b). *Nato3* continues to be expressed at similar levels in the midbrain of young (1-month-old), adult (4-month-old) and aged (14-month-old) mice (Fig. 5c). Immunohistochemistry analysis of coronal midbrain sections of 14-month-old mice based on anti-TH and anti-NATO3 antibodies revealed the presence of NATO3 in DA neurons of both the ventral tegmental area (VTA) and the SN, as well as in non-TH-positive cells (Fig. 5d), consistent with the RT-qPCR data.

Having verified the expression of *Nato3* in adult mDA neurons, we sought to conditionally delete *Nato3* in postmitotic DA neurons and investigate its consequences to dopamine-related behavior and the integrity of mDA neurons. We generated a mouse strain

bearing the *loxP*-flanked (floxed) allele of *Nato3* and crossed it with the *DAT-Cre* mouse expressing the Cre recombinase under the control of the dopamine transporter gene (*Slc6a3*) regulatory sequences[52]. *DAT-Cre* expression is known to arise postnatally in differentiated midbrain DA neurons, has no deleterious effects on DA neurons, and does not alter locomotion or anxiety-related behaviors[52,53]. We obtained homozygous *Nato3*-floxed animals harboring either no copies ($Nato3^{floxed}$, referred to as control) or one copy of the *DAT-Cre* transgene ($Nato3^{DAT\text{-}Cre}$, referred to as *Nato3* cKO) (Fig. 6a). RT-qPCR analysis of the ventral midbrain confirmed the ablation of *Nato3* in $Nato3^{DAT\text{-}Cre}$ mice (Fig. 6b).

We analyzed control and *Nato3* cKO mice at different ages using assays for dopamine-related behaviors. In the pole test, which is a sensitive assay for motor impairment associated with reduced striatal dopamine in rodents[54], *Nato3* cKO mice took significantly longer to turn and descend the pole than control mice at 13 months, while no difference was observed in younger animals (Fig. 6d). This observation indicates an age-dependent decline in motor coordination in *Nato3* cKO mice. Spontaneous activity levels measured via voluntary wheel running over three days were similar between *Nato3* cKO and control mice until 13 months of age. However, the activity levels of *Nato3* cKO significantly declined at 16 months (Fig. 6e). In contrast, no differences were found between *Nato3* cKO and control mice in the open field test, which measures exploratory behavior when mice are placed in a novel environment[55] (Supplementary Fig. 4). These results indicate that *Nato3* ablation in postmitotic DA neurons lead to motor abnormalities in aged mice, possibly caused by an age-dependent decline in the nigrostriatal dopaminergic function.

Nato3 is required for the maintenance of mitochondrial integrity in midbrain DA neurons

To broadly assess the integrity of the nigrostriatal pathway, ventral midbrain and striatal

sections of 16- to 18-month-old mice were analyzed by anti-TH immunohistochemistry. The number of DA neuron cell bodies in the SN and VTA (Fig. 6f-g), as well as the density of TH^+ fibers in the striatum (Fig. 6h-i), did not show significant differences between control and *Nato3* cKO mice. Therefore, locomotor deficits in the *Nato3* cKO mice likely originate from functional impairments of DA neurons rather than an overt loss of cellular integrity.

Fer2 mutation impairs mitochondrial morphology selectively of DA neurons in the PAM cluster, which precedes the degeneration of PAM neurons and locomotor deficits in *Drosophila*[28]. To determine whether *Nato3* ablation also leads to mitochondrial abnormalities in DA neurons in mice, we first visualized mitochondria in the SN using the antibodies against mitochondrial cytochrome c oxidase subunit 4 (COX4). The mitochondria appeared more globular in DA neurons of the SN in old (16-18 months) *Nato3* cKO mice compared with age-matched controls (Fig. 7a). Quantification of mitochondrial circularity showed a statistically significant increase (i.e. an accumulation of rounder mitochondria) in *Nato3*-ablated DA neurons, confirming the visual impression (Fig. 7b). We further examined the ultrastructure and morphology of mitochondria in the SN using transmission electron microscopy. In TH-labeled neurons from control mice, most mitochondria (88%) appeared normal, showing a dense and uniform matrix and regularly distributed cristae (Fig. 7c, top panels, and Fig. 7d). Strikingly, a large fraction (46%) of mitochondria from *Nato3* cKO mice displayed an aberrant morphology, showing a reduced and patchy matrix density with few remaining cristae; in certain cases these mitochondria contained almost no cristae, presented white inclusions and appeared dysmorphic (Fig. 7c, bottom panels, and Fig. 7d). Mitochondria from TH-negative cells appeared normal in *Nato3* cKO mice, suggesting that the aberrant mitochondrial morphology was cell-autonomously induced by *Nato3* deletion in DA neurons (Fig. 7c, right bottom panel). Although mitochondrial size did not differ between the two genotypes, mitochondria from SN neurons in *Nato3* cKO mice were rounder than

those in the control (Fig. 7e). These results demonstrate that *Nato3* is required for the maintenance of mitochondrial integrity in the DA neurons of the SN.

DISCUSSION

Our results demonstrate that *Fer2* is a master regulator of a transcriptional network that maintains mitochondrial integrity in DA neurons in *Drosophila*. This property renders *Fer2* a potent dopaminergic neuroprotective factor against genetic and oxidative insults implicated in PD pathogenesis. Furthermore, we show that *Nato3*, a mammalian homolog of *Fer2*, is required for the maintenance of mitochondrial integrity in mDA neurons. Both *Fer2* and *Nato3* are developmental transcription factors for DA neurons that continue to be expressed throughout life, and their loss of function in differentiated DA neurons leads to locomotor deficits in aged animals. Our findings corroborate the critical role of developmental transcription factors in the lifelong maintenance of DA neurons and suggest the evolutionary conservation of transcriptional mechanisms for dopaminergic neuroprotection and mitochondrial integrity.

Drosophila Fer2 (*48 related 2*, CG5952) and its paralogs *Fer1* and *Fer3* were originally named for their similarity to the p48 subunit of the pancreas transcription factor 1 complex (PTF1) in the bHLH domain by the group of Yuh Nung Jan[56]. Independently, due to the similarity to mammalian Atonal within the bHLH domain, *Fer3* (CG6913) was named *Drosophila Nephew of Atonal 3* (*Dnato3*) by the group of Nissim Ben-Arie[57]. Ben-Arie's group also isolated a mouse homolog of *Dnato3* and named it *MNato3*[57]. Brian L Black's lab also independently isolated the same mouse gene and named it *Neuronal-twist* (*N-twist*), due to its high sequence similarly to *M-twist*[58]. It is puzzling that, whereas Jan's group has reported the expression of *Fer2* mRNA in the brain and ventral nerve cord (VNC) of the embryo and *Fer3* expression in the primordial midgut of the embryo[56], Ben-Arie's and

Black's groups have shown the expression of *Fer3* mRNA in the CNS of the embryo, which supports the idea that *Fer3* is the homolog of *Nato3*[58]. Notwithstanding this inconsistency, we argue that *Fer2* is a functional homolog of *Nato3* based on the following reasons. The fact that fewer DA neurons are generated in *Fer2* loss-of-function mutants[28] is strikingly similar to the observation that 30% fewer mDA neurons are formed in *Nato3* constitutive KO[32], suggesting that *Fer2* bears a proneural function similar to that of *Nato3*. FER2 bHLH domain shows a high similarity to that of NATO3 as well as to FER1 and FER3. Moreover, we have demonstrated here and in previous work[28] that DA neurons are the primary site of *Fer2* expression and function, and that both *Fer2* and *Nato3* are required for mitochondrial maintenance in differentiated DA neurons. Nevertheless, the possibility that *Fer3* may also have similar roles as *Fer2* in the development and maintenance of DA neurons cannot be excluded and is worthy of further investigation.

This study is the first to report the function of *Nato3* in differentiated mDA neurons in mice. *Nato3* is classically known as a neurogenic transcription factor, expressed in the floor plate cells in the developing mesencephalon and spinal cord[32,34]. Although *Nato3* expression in the spinal cord of postnatal and adult mice has been reported[59], we found here its presence in the mDA neurons of adult mice. By conditionally ablating *Nato3* in postmitotic DA neurons, we were able to distinguish the function of *Nato3* in mature mDA neurons, i.e. the maintenance of mitochondrial integrity, from its role in neurogenesis. Importantly, human *Nato3* is expressed almost exclusively in the SN among adult tissues. Thus, it is plausible that human *Nato3* also plays an important role in the mitochondrial maintenance in SN dopaminergic neurons.

The genesis, specification and differentiation of mDA neurons are governed by a complex web of transcription factors[60]. Whereas *Nato3* acts as an "early transcription factor" required for neurogenesis[32], it can also directly regulate *Lmx1b*, *Shh* and *Foxa2* and thereby

409 indirectly regulates the late transcription factor *Nurr1*[33,51]. Since *Lmx1b*, *Foxa2* and *Nurr1* are
410 neuroprotective transcription factors[9,12,13,19], *Nato3* might contribute to dopaminergic
411 neuroprotection by regulating these genes. However, none of the homologs of developmental
412 transcription factors for mDA neurons were found among *Fer2* downstream targets in adult
413 PAM neurons. Therefore, the gene regulatory networks for mDA neuron development and
414 adult mDA maintenance may be substantially different.

415 Identification of *Nato3* transcriptional targets and downstream molecular events in
416 differentiated mDA neurons will provide crucial information to understand the role of *Nato3*
417 in mitochondrial maintenance. While further studies are required to obtain such data, here we
418 have performed homologous experiments in *Drosophila*, i.e. identification of direct and
419 indirect targets of *Fer2* in DA neurons in the PAM cluster. An intersectional approach
420 combining ChIP-seq, whole-head RNA-seq and RNA-seq of isolated PAM neurons,
421 unequivocally identified 26 direct and over 100 indirect *Fer2* target genes expressed in PAM
422 neurons. Among *Fer2* indirect targets, genes involved in mitochondrial function and structure,
423 including those required for ETC complexes assembly, are remarkably enriched. Malfunction
424 of the ETC leads to ROS overproduction, which in turn induces mitochondrial DNA
425 mutations, alters membrane permeability and mitochondria morphology, and further damages
426 the ETC complexes, in a pathogenic self-reinforcing loop. Indeed, dysfunctions of the ETC,
427 particularly of Complex I, have been proposed as a leading mechanism of DA
428 neurodegeneration[61,62]. Thus, our molecular data are in accordance with the observation that
429 *Fer2*^{2} flies display an overt defect in mitochondrial networks[28]. It is noteworthy that *Sod2*,
430 which encodes mitochondrial superoxide dismutase, is also an indirect target of *Fer2*.
431 Consistent with this finding, *Sod2* overexpression partially rescues the loss of PAM neurons
432 in *Fer2*^{2} mutants. Furthermore, *Fer2* overexpression reverses mitochondrial abnormalities in
433 the PAM neurons of *park*^{1} mutants and prevents PAM neuron loss in genetic and toxin

models of PD. These results are in agreement with previous reports that *Sod2* and *Sod2*-mimetic agents are protective in cell and fly models of PD[63], and endorse the further exploration of *Sod2* as a potential therapeutic target for PD.

Among *Fer2* direct targets, we discovered six genes whose dysregulation induces a loss of PAM neurons. None of these genes have been previously related to the DA system or implicated in neuronal development or survival. Further studies are needed to clarify how these novel actors and their mammalian homologues contribute to the biology of DA neurons. The number of new genes implicated in PAM neuron survival may increase in the future, as our list of *Fer2* direct targets is likely not exhaustive. *Fer2* is a stress-responsive transcription factor that is upregulated by oxidative insult or possibly by other stressors[28]. Under such conditions FER2 may be recruited to and/or regulate different sets of target genes.

A large fraction of *Fer2* primary targets encode transcription factors or chromatin proteins. This positions *Fer2* at the vertex of multiple transcriptional cascades and suggests that *Fer2* orchestrates the expression of a broad set of secondary targets (Supplementary Fig. 3b). *Fer2* expression is restricted to PAM neurons and a few other cell clusters in the brain, and ubiquitous or even pan-neuronal constitutive overexpression of *Fer2* causes lethality (data not shown), indicating that genetic programs driven by *Fer2* are highly specific to PAM neurons.

PD progresses from the asymptomatic (preclinical) period to a stage with a variety of nonmotor symptoms and subtle motor impairments that do not meet diagnostic criteria (prodromal PD), before a definite diagnosis is reached[64]. Modeling in animals this latent phase of the disease would facilitate the development of disease-modifying therapies and the discovery of early PD biomarkers. We propose that *Nato3* cKO mice can serve as a relevant model for prodromal PD, presenting moderate motor deficits and quasi-normal mDA neurons that accumulate abnormal mitochondria. There is growing evidence that neurodegeneration in

PD is manifested after several risk factors, including genetic predisposition, toxin exposure and aging, interact to overcome protective compensatory mechanisms[65]. Future work is needed to determine whether exposing *Nato3* cKO mice to a second genetic or environmental insult exacerbates its PD-related phenotypes and trigger overt DA neurodegeneration.

The activation of neuroprotective transcription factors offers potent therapeutic opportunities, allowing to modulate multiple downstream pathways in parallel. Indeed, *Nurr1* and *Foxa2* gene delivery[19], *Nurr1* activators[66] and *En1* infusion[20] in rodent PD models have shown encouraging results. In light of our findings that *Fer2* confers neuroprotection in multiple fly PD models, it is tempting to speculate that the overexpression or activation of *Nato3* may protect mDA neurons from genetic and environmental insults in mammals, with potential far-reaching implications for PD treatment.

METHODS

Drosophila stocks and maintenance

The following lines were obtained from the Bloomington *Drosophila* Stock Center (BDSC) (Indiana University, Bloomington, IN): *UAS-RedStinger* (#8546), *UAS-Sod2* (#24494), *park*^{1} (#34747), and *hs-GAL4* (#1799). *Fer2::GFP::V5*, *PBac{RB}Fer2*^{e03248} (referred to as *Fer2*^{1}), *Mi{ET1}Fer2*^{MB09480} (referred to as *Fer2*^{2}), *Fer2-GAL4, R58E02-GAL4*, *UAS-mitoGFP*, and *UAS-Fer2::FLAG* lines were previously described[26,28,67]. *UAS-Lrrk WT* and *UAS-Lrrk I1915T* were a kind gift from Yuzuru Imai[68]. All of the lines used to overexpress or knock-down *Fer2* primary targets are described in the Supplementary Table 3. All flies were maintained on standard cornmeal-agar food at 25 °C in a 12 h:12 h light-dark cycle and under controlled humidity.

Fly brain immunohistochemistry

Immunostaining of whole fly brains was performed as previously described[28]. Briefly, the flies were decapitated, and the heads were fixed in 4% paraformaldehyde (PFA) + 0.3% Triton X-100 for 1 h on ice and washed three times with PBST-0.3 (PBS, 0.3% Triton X-100). The cuticle was partially removed, and the partly opened heads were incubated with blocking solution (5% normal goat serum, PBS, 0.3% Triton X-100) for 1 h at room temperature (RT) on a rocking platform. Subsequently, the samples were incubated with primary antibodies for 48 h at 4 °C. After three 20 min washes with PBST-0.3, the samples were then incubated with Alexa Fluor-conjugated secondary antibodies overnight at 4 °C. After three 20 min washes with PBST-0.3, the remaining cuticle and trachea were removed and the brains were mounted in Vectashield medium (Vector Laboratories). Primary antibodies and the dilution factors were as follows: rabbit polyclonal anti-TH (ab152, Millipore) 1:100, polyclonal rabbit anti-GFP (A6455, Invitrogen) 1:250. Neuropil was counterstained with the mouse monoclonal antibody nc82 (Developmental Studies Hybridoma Bank) 1:100 to visualize the entire brain and assess its integrity. Secondary antibodies and the dilution factors were as follows: goat anti-rabbit IgG Alexa Fluor 488 conjugate (A-11034, Thermo Fisher Scientific) 1:250, goat anti-mouse IgG Alexa Fluor 633 conjugate (A-21052, Thermo Fisher Scientific) 1:250.

Mouse brain immunohistochemistry

Animals were anesthetized and perfused through the left ventricle with 0,2% Heparin in PBS at RT followed by ice-cold 10% formalin solution (Sigma HT501128-4L). The brains were dissected and post-fixed for 72 h in fresh 4% PFA (Thermo Fisher Scientific #28906) before being embedded in low melting point agarose (Thermo Fisher Scientific #R0801) and sectioned in a sliding vibratome at a thickness of 40 µm. Striatum sections were stained as floating sections. Ventral midbrain sections were adhered to the SuperFrost plus slides

(Thermo Fisher Scientific J1800AMNZ) before staining. Slices were incubated in blocking buffer (4% non-fat milk, 4% Bovine Serum Albumin (BSA), PBS) containing 0,1% Triton X-100 for 30 min at RT. The sections were then incubated with primary antibodies in blocking buffer containing 0,1% Tween for 48 h at 4 °C. After three 30 min washes in washing buffer (0.1% Tween, PBS), sections were incubated with the corresponding secondary antibody overnight at 4 °C, in the dark. After three 30 min washes in washing buffer, the slices were mounted with DABCO-glycerol mounting medium (25 mg/ml DABCO (Sigma D27802-25G), 90% glycerol, PBS; pH 8,6). For nuclear staining, prior to mounting midbrain slices were treated with 100µg/ml RNAse A (#EN0531, Thermo Fisher Scientific) for 30 min at 37 °C, and then incubated with TO-PRO-3 iodide (T3605, Sigma) for 30 min at RT. Primary antibodies and dilution factors were as follows: rabbit polyclonal anti-TH (Millipore ab152) 1:300, mouse anti-TH (Immunostar 22941) 1:300, rb polyclonal anti-NATO3 (Aviva ARP37423_P050) 1:70, mouse anti-COX4 (Thermo Fisher Scientific 1D6E1A8) 1:300. Secondary antibodies and dilution factors were the same as those for the fly brain immunostaining.

Microscopy and image analysis

Fly brains and mouse brain slices were scanned using a Leica TCS SP5 confocal microscope. Image analysis was performed using Fiji software[69]. All analyses were conducted blindly with respect to genotype.

Fly brain. TH-positive neurons were counted manually from Z-stacks of confocal images using the cell counter plugin of Fiji. PAM neuron counts were scored blindly. FER2::V5::GFP and TH fluorescence intensity in the PAM region was measured on Z-SUM projection images. The region of interest (ROI) corresponding to the PAM cluster was manually drawn to include TH^+ neurons. Background signal measured outside the ROI was

subtracted from the ROI signal. To quantify mitochondria circularity in PAM clusters, mitoGFP-positive objects within the PAM neurons region were analyzed using a particle analysis plugin as described previously[29].

Mouse brain. TH immunoreactivity in striatal regions was quantified by optical densitometry using Fiji. Three striatum images were acquired for each animal, and in every picture fluorescence intensity was measured for four squares drawn on the dorsal striatum (n=3-4 animals per genotype). Measures from all the squares were averaged to give the value for each animal. To obtain the number of mDA neurons, TH-positive neurons were counted manually from Z-stacks of confocal images using the cell counter plugin (n=3 animals per genotype). Every fourth section covering the entire VTA and SN in one brain hemisphere was included in the counting procedure. Neuron counts were scored blindly. To quantify mitochondria circularity in DA neurons, COX4-positive objects within the TH-positive DA neurons were analysed using the particle analysis plugin.

Treatment of flies with oxidative reagents

7-day-old flies were placed into empty vials and starved for 6 h. The flies were then transferred into vials containing *Drosophila* instant food (Formula 4-24 Instant Drosophila Medium, Carolina Biological Supply Company, USA) containing 5% H_2O_2 (Sigma, H1009), or vials containing *Drosophila* instant food only as a control, and kept for 24 h. All vials were kept in a humid box at 25 °C during the treatment. Following the treatment, flies were transferred back to the vials with standard cornmeal-agar food and maintained normally. Seven days after the treatment the flies were decapitated, and anti-TH-staining was performed as described above.

ROS detection

The level of ROS production in the fly brain was measured using a cell-permeable probe, 2'7'-dichlorofluorescin diacetate (H2DCF), following the protocol described in[70]. The fluorescence intensity for the entire central brain was measured using Fiji software[69] after generating a Z-SUM projection across the corresponding Z-stacks, as previously described[28].

Startle-induced climbing assay

For each experimental group, 20 male flies were briefly anesthetized with CO_2 and placed into a 100 ml graduated glass cylinder, which was divided into five equal parts marked 1-5 from bottom to top. Flies were left to recover from the CO_2 exposure for 1 h before the assay. The climbing assay was performed at ZT2 (2 h after lights-on in 12 h:12 h light-dark cycles) to avoid circadian variations in the locomotor activities of the flies, following the procedure previously described[28]. Briefly, the cylinder was tapped on a flexible pad to collect all of the flies at the bottom, and then the flies were allowed to climb up the wall of the cylinder for 20 s. The number of flies that climbed up to each zone within 20 s was counted manually and used to calculate the climbing index (CI) with the following formula: $CI = (0 \times n_0 + 1 \times n_1 + 2 \times n_2 + 3 \times n_3 + 4 \times n_4 + 5 \times n_5) / n_{total}$, where n_x is the number of flies that reached zone X, n_0 is the number of flies that remained in the bottom of the cylinder, and n_{total} is the total number of flies. Each experiment consisted of three trials, and three independent experiments were performed for each genotype. The mean CI values from three independent experiments are shown.

Chromatin immunoprecipitation coupled to sequencing (ChIP-seq)

ChIP was performed based on previous protocols[71,72] on *Fer2*^{1} mutant flies expressing a GFP::V5-tagged *Fer2* genomic transgene (*Fer2::GFP::V5*) and on *w*^{1118} flies (negative control). Briefly, ~8000 14-day-old flies per sample were collected 2 h before lights-on

584 (ZT22), frozen in liquid nitrogen and maintained at -80 °C until processed. Heads were
585 collected using metal sieves, and then, 1 ml of heads was ground in liquid nitrogen and
586 homogenized 30 times in 5 ml of NE Buffer (15 mM HEPES pH 8, 10 mM KCl, 0.1 mM
587 EDTA, 0.5 mM EGTA, 350 mM sucrose, 0.1% Tween 20, 5 mM MgCl2, 1 mM DTT, 1 mM
588 PMSF plus Protease inhibitor cocktail (Roche 11 873 580 001)) with 1% PFA. Fixation was
589 performed for 10 min at RT and quenched with 125 mM glycine for 5 min at RT. The
590 homogenate was filtered through a 100 µm nylon mesh filter (Thermo Fisher Scientific
591 22363549), and nuclei were collected by centrifugation at 800 x g for 5 min at 4 °C. The
592 nuclei were washed three times, resuspended in 1,5 ml of cold RIPA buffer (25 mM Tris-HCl
593 pH 8, 150 mM NaCl, 0,5% sodium deoxycholate, 0,1% SDS, 1% NP-40, 0,5 mM DTT plus
594 Protease inhibitor cocktail) and sonicated using a Bioruptor sonicator for 18 min (30 s ON/30
595 s OFF). The sonicated chromatin was then centrifuged at 10000 x g for 10 min at 4 °C to
596 remove cell debris. The supernatant was pre-cleared with agarose beads (1 h, 4 °C) and
597 incubated with 50 µl of saturated anti-V5 beads (Sigma A7345) overnight at 4 °C. The beads
598 were washed twice with low-salt buffer (20 mM Tris pH 8, 150 mM NaCl, 2 mM EDTA,
599 0,1% SDS, 1% Triton X-100), twice with high-salt buffer (20 mM Tris pH 8, 500 mM NaCl,
600 2 mM EDTA, 0,1% SDS, 1% Triton X-100), twice with LiCl buffer (10 mM Tris pH 8, 250
601 mM LiCl, 1 mM EDTA, 1% sodium deoxycholate, 1% NP-40) and twice with TE buffer (10
602 mM Tris-HCl pH 8, 1 mM EDTA). DNA was eluted in the V5 elution buffer (10 mM HEPES,
603 1,5 mM MgCl2, 0,25 mM EDTA, 20% glycerol, 250 mM KCl, 0,3% NP-40, 0,5 mg/ml V5
604 peptide) and incubated with RNase (30 min, 37 °C) and proteinase K (overnight, 65 °C).
605 Subsequently, the DNA was purified with a MinElute PCR purification kit (Qiagen 28004).
606 Libraries were prepared with 0,5 to 0,7 ng of ChIP-enriched DNA as starting material and
607 processed using the Illumina TruSeq ChIP kit according to the manufacturer's specifications,
608 at the iGE3 Genomics Platform in Geneva. The libraries were validated on a Tapestation

2200 (Agilent) and a Qubit fluorometer (Invitrogen - Thermo Fisher Scientific). Single reads of 50 bp were generated using the TruSeq SBS HS v3 chemistry on an Illumina HiSeq 2500 sequencer.

ChIP-seq analysis

Sequencing reads were mapped to the *Drosophila melanogaster* genome reference dm3 using Bowtie2 with default settings[73]. *Fer2* binding sites were identified by individually comparing each FER2 ChIP sample (N=2) to each w^{1118} ChIP sample (N=2; negative control) using MACS2[74]. The minimum FDR (q-value) cutoff for peak detection was 0.05. The 267 shared peaks overlapping in all the four FER2 ChIP vs w^{1118} ChIP comparisons were selected as confident peaks. Peak calling was also performed using Homer[75] and over 90% of Homer peaks overlapped with MACS2 peaks, confirming our results. ChIP-seq profiles were visualized using IGV[76]. HOMER motif analysis algorithm was used to search for enriched motifs, and identified a 12-mer containing a bHLH binding site, present in the majority of the best ranked peaks. Peak-to-gene assignment was performed using the HTSstation[77] and resulted in a list of 279 genes.

Whole-head RNA-seq

hs-GAL4, *UAS-Fer2::FLAG* flies (*hs>Fer2::FLAG*) were heat-shocked at 37 °C for 3 h, or maintained at 25 °C (control), and collected 12 h or 48 h later (three independent biological replicates per group). The same procedure was also applied to flies carrying *hs-GAL4* but not the *UAS-Fer2,* in order to identify and exclude from our analysis the genes that responded to heat irrespective of *Fer2* induction. The flies were frozen in liquid nitrogen and kept at -80 °C until processed. Fly heads were collected using metal sieves and kept in Trizol (Life Technologies 15596026) at -80 °C until processed. Total RNA was isolated from dissected

mouse brain regions using Trizol according to the manufacturer's instructions and treated with Turbo DNase for 30 min at 37 °C (Turbo DNA-free kit, Thermo Fisher Scientific AM1907). Libraries were prepared at the iGE3 Genomics Platform in Geneva. Single reads of 50 bp were generated using an Illumina HiSeq 2500 sequencer. Data analysis was performed using Galaxy[78]. Sequencing reads were mapped to the *Drosophila melanogaster* genome reference dm3 using TopHat[79] with default settings. Differentially expressed genes (DEG) analysis was performed with Cufflinks, Cuffmerge and Cuffdiff, to compare flies who received the heat shock treatment with control flies kept at 25 °C. The same analysis was performed on *hs-GAL4* flies, to identify the genes which responded to heat irrespective of *Fer2* induction. These heat-responsive genes were subtracted from DEG identified in the *hs>Fer2::FLAG* experiment.

PAM-specific RNA-seq

Flies carrying *R58-GAL4* were combined with *UAS-Fer2::FLAG* to overexpress *Fer2*, and with *UAS-RedStinger* to mark PAM neurons. Flies carrying only *R58-GAL4* and *UAS-RedStinger* were used as a control. Cells were dissociated from the brains of ~70 14-day-old flies 2 h before lights-on (ZT22) as previously described[67], except that the brains were treated with papain for 25 min. After trituration in 300 µl SMactive medium containing 50 µm AP5, 20 µm DNQX and 0.1 µm TTX, the cell suspension was filtered through a sterile 70 µm membrane and distributed to three wells of three two-well chamber glass slides (LabTek II, Nunc) kept on ice. The second well of each slide contained ice to cool the cells while RedStinger-positive cells were sorted on a fluorescence microscope equipped with a motorized stage and a needle holder (CellSorter Company for Innovations). Cells were selected manually using capillaries with 50 µm tip diameter. Collected cells were released in a clean part of the chamber and immediately picked up again, greatly reducing the amount of

debris, before being transferred to a fresh slide with 100 µl medium spread in a 1 × 1 cm GeneFrame (Thermo Fisher Scientific). Cells were reselected for two rounds and finally transferred using a new capillary with 30-µm tip diameter to 100-µl lysis buffer (Absolutely RNA Nanoprep Kit; Agilent). Cells of multiple collections were pooled if needed to obtain 200 cells per sample, and total RNA was extracted according to the manufacturer's instructions. The RNA was converted to cDNA and amplified using the SMART-Seq4 Kit (Takara Bio). Libraries were generated using NexteraXT (Illumina) and sequenced on an Illumina HiSeq 2500 or 4000. DEG analysis was performed using the HTSstation[77] and resulted in a list of 132 genes.

Bioinformatic analysis of genes found in ChIP-seq and RNA-seq

Since human databases are generally more comprehensive, fly genes were converted into human orthologs prior to Gene Ontology (GO) analysis[80]. Human orthologs of fly genes were predicted using DIOPT[81] and were analyzed for GO with Metascape[80]. A network representation of GO terms was obtained using Cytoscape[82]. A search for TF binding sites enriched among promoters of PAM-specific RNAseq DEG was performed using PSCAN[83]. Protein-protein interactions were investigated using STRING[84] and a previously reported *Drosophila* TFs database [48].

Mice strains

Nato3-LoxP mice was generated using Clustered Regularly Interspaced Short Palindromic Repeats (CRISPR) technology by Applied StemCell, Inc. (Milpitas, CA). Two copies of a synthetic *LoxP* sequence were inserted upstream and downstream of the unique exon of *Nato3* gene. Briefly, a mixture of active guide RNA molecules (gRNAs), two single stranded oligo donor nucleotides (ssODNs) and *Cas-9* mRNA was prepared and injected into the

cytoplasm of C57BL/6 embryos. Mice born from the microinjection were screened to identify *LoxP* insertions at the designated locations using PCR and sequencing. The founder mice were bred to evaluate the germline transmission and expand the *Nato3-LoxP* colonies. *DAT-Cre* mice have been described previously[52] (obtained from Jean-Claude Martinou's laboratory, University of Geneva). *DAT-Cre* and *Nato3-LoxP* mice were maintained in a C57BL/6J genetic background. Crosses between these lines generated mice that are homozygous for the *Nato3-LoxP* allele and harbor one copy of the *DAT-Cre* transgene ($Nato3^{DAT\text{-}Cre}$). Littermates homozygous for *Nato3* floxed alleles and harboring no copy of the *DAT-Cre* transgene were used as controls ($Nato3^{floxed}$). Mice were maintained in rooms with controlled 12 h light/dark cycles, temperature and humidity, with food and water provided *ad libitum*. Mice were housed at a maximum of five animals per cage in individually ventilated cages. All experiments were conducted in accordance with the Institutional Animal Care and Use Committee of the University of Geneva and with permission of the cantonal authorities (Permit No. GE/3/19 27381 and GE/78/19 31317).

Electron microscopy image acquisition and analysis

Animals were anesthetized, perfused and embedded in agarose as described in the mouse brain immunohistochemistry section, except that the perfusion was performed with 3% PFA complemented with 0.2% glutaraldehyde in 0.1 M phosphate buffer (PB), pH 7.4. Subsequently, 60 µm-thick sections were cut and processed for pre-embedding immunoperoxidase staining, as previously described [85]. Briefly, immunostaining for DA neurons in the SN was performed by incubating the sections with rabbit anti-TH antibodies (Millipore ab152, 1:100) followed by goat anti-rabbit biotinylated secondary antibodies (Vector Laboratories PK-4001, 1:200) and then avidin biotin peroxidase complex (Vector Laboratories PK-4001). 3,3'-diaminobenzidine tetrachloride (DAB; Invitrogen Life

Technologies 750118) was applied for 1-2 minutes until the stain developed. Sections were further embedded in EPON resin (Fluka) and trimmed around the labeled cells of interest. Ultrathin (60 nm) sections were produced and imaged by a Tecnai G212 electron microscope (FEI Company, Oregon, United states) equipped with a digital camera (Mega View III; Soft Imaging Systems). ~15 labeled cells from two mice were analyzed for each genotype. Mitochondria were classified blindly. Mitochondrial size and roundness were measured via Fiji software using the particle analysis plugin after a manual selection of each mitochondrion.

RT-qPCR on mouse brain regions

Animals were sacrificed by cervical dislocation and decapitated. The brains were immediately removed and all the subsequent steps were performed on ice. The olfactory bulbs, prefrontal cortex, striatum, cortex, and cerebellum were scalpel-dissected. The ventral and dorsal midbrain were scalpel-dissected from 1 mm-thick brain slices cut in an ice-cold coronal matrix (Zivic Instruments). Samples were kept in Trizol (Life Technologies 15596026) at -80 °C until processed. Total RNA was isolated from dissected mouse brain regions using Trizol according to the manufacturer's instructions and treated with Turbo DNase for 30 min at 37 °C (Turbo DNA-free kit, Thermo Fisher Scientific AM1907). Reverse transcription was performed from 500 to 1000 ng RNA using the Maxima reverse transcriptase (Thermo Fisher Scientific 18090050) and oligo-dT primers, according to the manufacturer's instructions. Primers were designed with Primer-BLAST online tool (https://www.ncbi.nlm.nih.gov/tools/primer-blast/): *B2m* (F: 5'-AGAATGGGAAGCCGAACATA, R: 5'-CGTTCTTCAGCATTTGGATT), *Cyclophilin* (F: 5'-TGCCATCCAGCCAGGAGGTC, R: 5'-CCATCGTGTCATCAAGGACTT), *Hmbs* (F: 5'-GCTGAAAGGGCTTTTCTGAG, R: 5'-TGCCCATCTTTCATCACTGT), *Hprt1* (F: 5'-TGTCAGTTGCTGCGTCCCCAGA, R: 5'-TCTACCAGAGGGTAGGCTGGCC), *Pgk1*

(F: 5'-ACCTGCTGGCTGGATGGGCT, R: 5'-CTCGACCCACAGCCTCGGCA), *Rpl13a* (F: 5'-CGGATGGTGGTCCCTGCTG, R: 5'-GAGTGGCTGTCACTGCCTGG), *Nato3* (F: 5'-GGTGAGCCCAAGAGACACTC, R: 5'-GTGCCGGATCCCCAACTTAT). Quantitative PCR (qPCR) was performed on the Light Cycler LC480 (Roche) using the TB Green Ex Taq II polymerase (Takara RR820L). Each reaction was performed in triplicate. Relative quantification and normalization were performed with a multiple reference genes model[86]. For normalization, the best reference genes for each experiment were determined using the geNorm algorithm (https://genorm.cmgg.be) within a panel of 4-5 putative reference genes. To compare *Nato3* levels between different brain regions, *B2m* and *cyclophilin* were used as reference genes. To compare *Nato3* levels in the midbrain between different ages, *B2m* and *Hprt1* were used.

Behavioral tests

Male mice of different ages (7, 10, 13 and 16 months) were evaluated for posture control and coordination (pole test), spontaneous locomotor activity (wheel test) and exploration-driven locomotor behavior (open field test). All behavioral tests were performed during the light cycle by experimenters blind to the genotype. The mice were allowed to habituate to the behavioral room for at least 45 min before each test. Behavioral equipment was cleaned with 70% ethanol after each test session to avoid olfactory cues.

Pole test. The pole test was performed as previously described[54] with minor modifications. Mice were first trained 4-6 times by placing the animal head-down on top of a vertical pole (diameter: 1 cm, height: 55 cm) and letting it descend. Then, animals were trained 3-4 times in the regular turning and descending procedure, by placing the animal head-up on top of the pole. For the actual test, mice performed eight trials and were recorded with a video camera. The time to orient downward (T-turn) and the total time to turn and

descend the pole (T-tot) were measured, with a maximum duration of 30 s. When the mouse was not able to turn downward and instead dropped from the pole in a lateral body position, a value of 30 s was assigned. The average of the eight trials was used as the final score. During the training and for the real test, mice were tested a maximum of three times per day, with an interval of at least 5 min between trials.

Running wheel test. Mice were singly housed in cages with free access to a running wheel (14 cm in diameter) for 6 days, under a 12 h light/dark cycles. After three days of habituation, the number of wheel revolutions per minute was recorded with a sensor by LabVIEW program for the following three days. The total amount of time spent on the wheel and the total distance run were calculated for each animal.

Open field test. Open field test was performed as previously described[13] with minor modifications. The test was performed in a 40 x 40 x 40 cm arena made of white Plexiglas plastic, which was illuminated from above (light intensity of 100 lux on the floor). Mice were placed individually in the center of the area and allowed to freely explore it for 10 min while being recorded. The horizontal locomotor activity was analyzed using the Mouse Behavioral Analysis Toolbox (MouBeAT)[87] for ImageJ. The vertical activity (rearing), defined as a mouse rising on its hind legs, was scored manually.

Statistical analysis

Statistical comparisons were performed using GraphPad Prism software (San Diego, CA). The statistical significance of differences between two groups was calculated using a nonparametric two-tailed Mann-Whitney test. To compare three or more groups, ANOVA followed by Turkey's multiple comparisons test was used. For the circularity analysis, to compare the distribution of mitochondria particles between two or three genotypes, the Kolmogorov-Smirnov test and the Kruskal-Wallis test followed by Dunn's test were applied,

respectively. Differences were considered significant at *p<0.05, **p<0.01, ***p<0.001, ****p<0.0001.

ACKNOWLEDGMENTS

We thank Ernst Hafen, Chi-Hon Lee, Junhai Han, the Bloomington *Drosophila* Stock Center, the Vienna Drosophila Resource Center and the Kyoto Stock Center for fly stocks, J-C. Martinou for the *DAT-Cre* mouse strain. We thank the Genomics Platform of iGE3 for ChIP-seq and RNA-seq experiments, the animal facility of the University of Geneva for maintenance of mice colonies, and the Pole Facultaire de Microscopie Electronique (Centre Médical Universitaire, Geneva) for electron microscopy. We are grateful to J-C. Martinou and our lab members for valuable discussions of this work. This research was supported by the European Research Council (ERC-StG-311194), the Swiss National Science Foundation (31003A_130387), the Georges and Antoine Claraz Foundation, the Novartis Foundation for Medical-Biomedical Research (19A025), the Société Académique de Genève, the Plan Stratégique Sciences Vie (PSVIE) of the University of Geneva, and the Canton of Geneva.

AUTHOR CONTRIBUTIONS

EN conceptualized the study. EN, FM, LS, DT and NL designed experiments. FM, DT, LS, NL, IN, MD, EV and PBD performed experiments and analyzed data. FM, DT, LS, MD, and EN produced visualizations of the results and made figures. FM and EN wrote the manuscript.

COMPETING INTERESTS

The authors have declared that no competing interests exist.

REFERENCES

1. Klein, M. O. *et al.* Dopamine: Functions, Signaling, and Association with Neurological Diseases. *Cell. Mol. Neurobiol.* **39**, 31–59 (2019).
2. Shulman, J. M., De Jager, P. L. & Feany, M. B. Parkinson's Disease: Genetics and Pathogenesis. *Annu. Rev. Pathol. Mech. Dis.* **6**, 193–222 (2011).
3. Connolly, B. S. & Lang, A. E. Pharmacological Treatment of Parkinson Disease: A Review. *JAMA* **311**, 1670 (2014).
4. Kalia, L. V. & Lang, A. E. Parkinson's disease. *The Lancet* **386**, 896–912 (2015).
5. Deng, H., Wang, P. & Jankovic, J. The genetics of Parkinson disease. *Ageing Res. Rev.* **42**, 72–85 (2018).
6. Haelterman, N. A. *et al.* A Mitocentric View of Parkinson's Disease. *Annu. Rev. Neurosci.* **37**, 137–159 (2014).
7. Von Stockum, S., Nardin, A., Schrepfer, E. & Ziviani, E. Mitochondrial dynamics and mitophagy in Parkinson's disease: A fly point of view. *Neurobiol. Dis.* **90**, 58–67 (2016).
8. Sonnier, L. *et al.* Progressive Loss of Dopaminergic Neurons in the Ventral Midbrain of Adult Mice Heterozygote for Engrailed1. *J. Neurosci.* **27**, 1063–1071 (2007).
9. Laguna, A. *et al.* Dopaminergic control of autophagic-lysosomal function implicates Lmx1b in Parkinson's disease. *Nat. Neurosci.* **18**, 826–835 (2015).
10. Doucet-Beaupré, H. *et al.* Lmx1a and Lmx1b regulate mitochondrial functions and survival of adult midbrain dopaminergic neurons. *Proc. Natl. Acad. Sci.* **113**, E4387–E4396 (2016).
11. Kittappa, R., Chang, W. W., Awatramani, R. B. & McKay, R. D. G. The foxa2 Gene Controls the Birth and Spontaneous Degeneration of Dopamine Neurons in Old Age. *PLoS Biol.* **5**, e325 (2007).
12. Domanskyi, A., Alter, H., Vogt, M. A., Gass, P. & Vinnikov, I. A. Transcription factors Foxa1 and Foxa2 are required for adult dopamine neurons maintenance. *Front. Cell. Neurosci.* **8**, (2014).
13. Kadkhodaei, B. *et al.* Transcription factor Nurr1 maintains fiber integrity and nuclear-encoded mitochondrial gene expression in dopamine neurons. *Proc. Natl. Acad. Sci.* **110**, 2360–2365 (2013).
14. van den Munckhof, P. *et al.* Pitx3 is required for motor activity and for survival of a subset of midbrain dopaminergic neurons. *Dev. Camb. Engl.* **130**, 2535–2542 (2003).
15. Di Salvio, M. *et al.* Otx2 controls neuron subtype identity in ventral tegmental area and antagonizes vulnerability to MPTP. *Nat. Neurosci.* **13**, 1481–1488 (2010).
16. Blaudin de Thé, F. *et al.* Engrailed homeoprotein blocks degeneration in adult dopaminergic neurons through LINE□1 repression. *EMBO J.* **37**, (2018).
17. Le, W. *et al.* Mutations in NR4A2 associated with familial Parkinson disease. *Nat. Genet.* **33**, 85–89 (2003).
18. Bergman, O. *et al.* Do polymorphisms in transcription factors LMX1A and LMX1B influence the risk for Parkinson's disease? *J. Neural Transm.* **116**, 333–338 (2009).
19. Oh, S. *et al.* Combined Nurr1 and Foxa2 roles in the therapy of Parkinson's disease. *EMBO Mol. Med.* **7**, 510–525 (2015).
20. Alvarez-Fischer, D. *et al.* Engrailed protects mouse midbrain dopaminergic neurons against mitochondrial complex I insults. *Nat. Neurosci.* **14**, 1260–1266 (2011).
21. Di Giovannantonio, L. G. *et al.* Otx2 selectively controls the neurogenesis of specific neuronal subtypes of the ventral tegmental area and compensates En1-dependent neuronal loss and MPTP vulnerability. *Dev. Biol.* **373**, 176–183 (2013).
22. Hewitt, V. L. & Whitworth, A. J. Mechanisms of Parkinson's Disease. in *Current Topics in Developmental Biology* vol. 121 173–200 (Elsevier, 2017).

23. Nagoshi, E. Drosophila Models of Sporadic Parkinson's Disease. *Int. J. Mol. Sci.* **19**, 3343 (2018).
24. Landayan, D. & Wolf, F. W. Shared neurocircuitry underlying feeding and drugs of abuse in Drosophila. *Biomed. J.* **38**, 496–509 (2015).
25. Strausfeld, N. J. & Hirth, F. Deep Homology of Arthropod Central Complex and Vertebrate Basal Ganglia. *Science* **340**, 157–161 (2013).
26. Liu, C. *et al.* A subset of dopamine neurons signals reward for odour memory in Drosophila. *Nature* **488**, 512–516 (2012).
27. Riemensperger, T. *et al.* A Single Dopamine Pathway Underlies Progressive Locomotor Deficits in a Drosophila Model of Parkinson Disease. *Cell Rep.* **5**, 952–960 (2013).
28. Bou Dib, P. *et al.* A Conserved Role for p48 Homologs in Protecting Dopaminergic Neurons from Oxidative Stress. *PLoS Genet.* **10**, e1004718 (2014).
29. Tas, D. *et al.* Parallel roles of transcription factors dFOXO and FER2 in the development and maintenance of dopaminergic neurons. *PLOS Genet.* **14**, e1007271 (2018).
30. Lawal, H. O. *et al.* The Drosophila vesicular monoamine transporter reduces pesticide-induced loss of dopaminergic neurons. *Neurobiol. Dis.* **40**, 102–112 (2010).
31. Sun, J. *et al.* Neural Control of Startle-Induced Locomotion by the Mushroom Bodies and Associated Neurons in Drosophila. *Front. Syst. Neurosci.* **12**, 6 (2018).
32. Y. Ono, Nakatani, T., Minaki, Y. & Kumai, M. The basic helix-loop-helix transcription factor Nato3 controls neurogenic activity in mesencephalic floor plate cells. *Development* **137**, 1897–1906 (2010).
33. Nissim-Eliraz, E., Zisman, S., Schatz, O. & Ben-Arie, N. Nato3 Integrates with the Shh-Foxa2 Transcriptional Network Regulating the Differentiation of Midbrain Dopaminergic Neurons. *J. Mol. Neurosci.* **51**, 13–27 (2013).
34. Mansour, A. A., Khazanov-Zisman, S., Netser, Y., Klar, A. & Ben-Arie, N. Nato3 plays an integral role in dorsoventral patterning of the spinal cord by segregating floor plate/p3 fates via Nkx2.2 suppression and Foxa2 maintenance. *Development* **141**, 574–584 (2014).
35. Zimprich, A. *et al.* Mutations in LRRK2 Cause Autosomal-Dominant Parkinsonism with Pleomorphic Pathology. *Neuron* **44**, 601–607 (2004).
36. Langston, R. G., Rudenko, I. N. & Cookson, M. R. The function of orthologues of the human Parkinson's disease gene LRRK2 across species: implications for disease modelling in preclinical research. *Biochem. J.* **473**, 221–232 (2016).
37. Kitada, T. *et al.* Mutations in the parkin gene cause autosomal recessive juvenile parkinsonism. *Nature* **392**, 605–608 (1998).
38. Cha, G.-H. *et al.* Parkin negatively regulates JNK pathway in the dopaminergic neurons of Drosophila. *Proc. Natl. Acad. Sci.* **102**, 10345–10350 (2005).
39. Park, J. *et al.* Mitochondrial dysfunction in Drosophila PINK1 mutants is complemented by parkin. *Nature* **441**, 1157–1161 (2006).
40. Park, J., Lee, G. & Chung, J. The PINK1–Parkin pathway is involved in the regulation of mitochondrial remodeling process. *Biochem. Biophys. Res. Commun.* **378**, 518–523 (2009).
41. Greene, J. C. *et al.* Mitochondrial pathology and apoptotic muscle degeneration in Drosophila parkin mutants. *Proc. Natl. Acad. Sci.* **100**, 4078–4083 (2003).
42. Clark, I. E. *et al.* Drosophila pink1 is required for mitochondrial function and interacts genetically with parkin. *Nature* **441**, 1162–1166 (2006).
43. Poole, A. C. *et al.* The PINK1/Parkin pathway regulates mitochondrial morphology. *Proc. Natl. Acad. Sci.* **105**, 1638–1643 (2008).
44. Scialò, F. *et al.* Mitochondrial ROS Produced via Reverse Electron Transport Extend Animal Lifespan. *Cell Metab.* **23**, 725–734 (2016).

45. Croset, V., Treiber, C. D. & Waddell, S. Cellular diversity in the Drosophila midbrain revealed by single-cell transcriptomics. *eLife* **7**, e34550 (2018).
46. Davie, K. *et al.* A Single-Cell Transcriptome Atlas of the Aging Drosophila Brain. *Cell* **174**, 982-998.e20 (2018).
47. Flynn, J. M. & Melov, S. SOD2 in mitochondrial dysfunction and neurodegeneration. *Free Radic. Biol. Med.* **62**, 4–12 (2013).
48. Shokri, L. *et al.* A Comprehensive Drosophila melanogaster Transcription Factor Interactome. *Cell Rep.* **27**, 955-970.e7 (2019).
49. Zhu, J., Chen, L., Sun, G. & Raikhel, A. S. The Competence Factor Ftz-F1 Potentiates Ecdysone Receptor Activity via Recruiting a p160/SRC Coactivator. *Mol. Cell. Biol.* **26**, 9402–9412 (2006).
50. Xie, X.-J. *et al.* CDK8-Cyclin C Mediates Nutritional Regulation of Developmental Transitions through the Ecdysone Receptor in Drosophila. *PLoS Biol.* **13**, e1002207 (2015).
51. Peterson, D. J. *et al.* The Basic Helix-Loop-Helix Gene Nato3 Drives Expression of Dopaminergic Neuron Transcription Factors in Neural Progenitors. *Neuroscience* **421**, 176–191 (2019).
52. Turiault, M. *et al.* Analysis of dopamine transporter gene expression pattern -- generation of DAT-iCre transgenic mice. *FEBS J.* **274**, 3568–3577 (2007).
53. Engblom, D. *et al.* Glutamate receptors on dopamine neurons control the persistence of cocaine seeking. *Neuron* **59**, 497–508 (2008).
54. Matsuura, K., Kabuto, H., Makino, H. & Ogawa, N. Pole test is a useful method for evaluating the mouse movement disorder caused by striatal dopamine depletion. *J. Neurosci. Methods* **73**, 45–48 (1997).
55. Gould, T. D., Dao, D. T. & Kovacsics, C. E. The open field test. in *Mood and anxiety related phenotypes in mice: Characterization using behavioral tests* 1–20 (Humana Press, 2009). doi:10.1007/978-1-60761-303-9_1.
56. Moore, A. W., Barbel, S., Jan, L. Y. & Jan, Y. N. A genomewide survey of basic helix-loop-helix factors in Drosophila. *Proc. Natl. Acad. Sci.* **97**, 10436–10441 (2000).
57. Segev, E., Halachmi, N., Salzberg, A. & Ben-Arie, N. Nato3 is an evolutionarily conserved bHLH transcription factor expressed in the CNS of Drosophila and mouse. *Mech. Dev.* **106**, 197–202 (2001).
58. Verzi, M. P. *et al.* N-twist, an evolutionarily conserved bHLH protein expressed in the developing CNS, functions as a transcriptional inhibitor. *Dev. Biol.* **249**, 174–190 (2002).
59. Khazanov, S. *et al.* Floor plate descendants in the ependyma of the adult mouse Central Nervous System. *Int. J. Dev. Biol.* **61**, 257–265 (2017).
60. Arenas, E., Denham, M. & Villaescusa, J. C. How to make a midbrain dopaminergic neuron. *Development* **142**, 1918–1936 (2015).
61. Vilain, S. *et al.* The Yeast Complex I Equivalent NADH Dehydrogenase Rescues pink1 Mutants. *PLoS Genet.* **8**, e1002456 (2012).
62. Pogson, J. H. *et al.* The complex I subunit NDUFA10 selectively rescues Drosophila pink1 mutants through a mechanism independent of mitophagy. *PLoS Genet.* **10**, e1004815 (2014).
63. Biosa, A. *et al.* Superoxide dismutating molecules rescue the toxic effects of PINK1 and parkin loss. *Hum. Mol. Genet.* **27**, 1618–1629 (2018).
64. Mahlknecht, P., Seppi, K. & Poewe, W. The Concept of Prodromal Parkinson's Disease. *J. Park. Dis.* **5**, 681–697 (2015).
65. Carvey, P. M., Punati, A. & Newman, M. B. Progressive dopamine neuron loss in Parkinson's disease: the multiple hit hypothesis. *Cell Transplant.* **15**, 239–250 (2006).

66. Spathis, A. D. *et al.* Nurr1:RXRα heterodimer activation as monotherapy for Parkinson's disease. *Proc. Natl. Acad. Sci. U. S. A.* **114**, 3999–4004 (2017).
67. Nagoshi, E. *et al.* Dissecting differential gene expression within the circadian neuronal circuit of Drosophila. *Nat. Neurosci.* **13**, (2010).
68. Imai, Y. *et al.* Phosphorylation of 4E-BP by LRRK2 affects the maintenance of dopaminergic neurons in Drosophila. *EMBO J.* **27**, 2432–2443 (2008).
69. Schindelin, J. *et al.* Fiji - an Open Source platform for biological image analysis. *Nat. Methods* **9**, (2012).
70. Owusu-Ansah, E., Yavari, A. & Banerjee, U. A protocol for in vivo detection of reactive oxygen species. *Protoc. Exch.* (2008) doi:10.1038/nprot.2008.23.
71. Meireles-Filho, A. C. A., Bardet, A. F., Yáñez-Cuna, J. O., Stampfel, G. & Stark, A. cis-regulatory requirements for tissue-specific programs of the circadian clock. *Curr. Biol. CB* **24**, 1–10 (2014).
72. Zhou, J., Yu, W. & Hardin, P. E. ChIPping away at the Drosophila clock. *Methods Enzymol.* **551**, 323–347 (2015).
73. Langmead, B. & Salzberg, S. L. Fast gapped-read alignment with Bowtie 2. *Nat. Methods* **9**, 357–359 (2012).
74. Feng, J., Liu, T., Qin, B., Zhang, Y. & Liu, X. S. Identifying ChIP-seq enrichment using MACS. *Nat. Protoc.* **7**, (2012).
75. Heinz, S. *et al.* Simple combinations of lineage-determining transcription factors prime cis-regulatory elements required for macrophage and B cell identities. *Mol. Cell* **38**, 576–589 (2010).
76. Robinson, J. T. *et al.* Integrative genomics viewer. *Nat. Biotechnol.* **29**, 24–26 (2011).
77. David, F. P. A. *et al.* HTSstation: A Web Application and Open-Access Libraries for High-Throughput Sequencing Data Analysis. *PLOS ONE* **9**, e85879 (2014).
78. Afgan, E. *et al.* The Galaxy platform for accessible, reproducible and collaborative biomedical analyses: 2018 update. *Nucleic Acids Res.* **46**, W537–W544 (2018).
79. Kim, D. *et al.* TopHat2: accurate alignment of transcriptomes in the presence of insertions, deletions and gene fusions. *Genome Biol.* **14**, R36 (2013).
80. Zhou, Y. *et al.* Metascape provides a biologist-oriented resource for the analysis of systems-level datasets. *Nat. Commun.* **10**, 1523 (2019).
81. Hu, Y. *et al.* An integrative approach to ortholog prediction for disease-focused and other functional studies. *BMC Bioinformatics* **12**, 357 (2011).
82. Shannon, P. *et al.* Cytoscape: a software environment for integrated models of biomolecular interaction networks. *Genome Res.* **13**, 2498–2504 (2003).
83. Zambelli, F., Pesole, G. & Pavesi, G. Pscan: finding over-represented transcription factor binding site motifs in sequences from co-regulated or co-expressed genes. *Nucleic Acids Res.* **37**, W247-252 (2009).
84. Szklarczyk, D. *et al.* STRING v11: protein-protein association networks with increased coverage, supporting functional discovery in genome-wide experimental datasets. *Nucleic Acids Res.* **47**, D607–D613 (2019).
85. Nikonenko, I. *et al.* PSD-95 promotes synaptogenesis and multiinnervated spine formation through nitric oxide signaling. *J. Cell Biol.* **183**, 1115–1127 (2008).
86. Hellemans, J., Mortier, G., De Paepe, A., Speleman, F. & Vandesompele, J. qBase relative quantification framework and software for management and automated analysis of real-time quantitative PCR data. *Genome Biol.* **8**, R19 (2007).
87. Bello-Arroyo, E. *et al.* MouBeAT: A New and Open Toolbox for Guided Analysis of Behavioral Tests in Mice. *Front. Behav. Neurosci.* **12**, 201 (2018).

FIGURE LEGENDS

Figure 1. *Fer2* overexpression prevents the loss of PAM dopaminergic neurons and mitochondrial dysfunction in genetic models of PD.

(a and b) *Fer2* overexpression prevented the loss of PAM neurons induced by the targeted expression of wild-type (*WT*) or pathogenic mutant *Lrrk* in PAM neurons. **(a)** Representative images of PAM neurons at day 14 detected by anti-TH antibodies (green). *PAM*, PAM neuron-specific *R58E02-GAL4* driver. *PAM>X* indicates that *UAS-transgene X* is driven by *R58E02-GAL4*. Scale bar, 20 μm. Top left, a schematic of DA neurons in the PAM (green) and other clusters (black). **(b)** Quantification of the number of PAM neurons per hemisphere. Box boundaries are the 25th and 75th percentiles, the horizontal line across the box is the median, and the whiskers indicate the minimum and maximum values. n=7-10 brains per group. **p<0.01, ***p<0.001, ****p<0.0001. n.s., not significant. One-way ANOVA followed by a Turkey's test for multiple group comparison. **(c and d)** *Fer2* overexpression in PAM neurons rescued PAM neuron loss in $Park^1$ mutants. Quantification of the number of PAM neurons per hemisphere in the indicated age and genotypes. n=7-10 brains per group. *p<0.05, **p<0.01, ***p<0.001, ****p<0.0001. n.s., not significant. One-way ANOVA followed by a Turkey's test for multiple group comparison (**c**) and Mann-Whitney test (**d**). **(e)** The mitochondrial network in PAM neurons was visualized using mitoGFP. Scale bar, 5 μm. **(f)** Top, histograms showing the circularity distribution of GFP^+ particles measured from (**e**). Bottom, the Gaussian curve fit to the circularity histogram. Circularity ranges from 0 (reticular mitochondria) to 1 (round mitochondria). The histogram of *PAM>mitoGFP,* $park^1$ is right-shifted compared with those of *PAM>mitoGFP,* $park^1$/+ and *PAM>mitoGFP, Fer2,* $park^1$, indicating the accumulation of rounder mitochondria in $park^1$ and its rescue by *Fer2*. ****p<0.0001 using Kruskal-Wallis test followed by Dunn's test for multiple group comparison. More than 500 mitochondrial particles were analyzed from 7-10 brains per

genotype.

Figure 2. *Fer2* overexpression protects PAM dopaminergic neurons from oxidative insults.

(a) w^{1118}, $Fer2^{2}/+$, $Fer2^{2}$, *R58E02-GAL4* (*PAM*) and PAM>*Fer2* flies were fed with H_2O_2 at day 7 for 24 h and the number of PAM neurons was examined at day 14. *Fer2* mutation exacerbates, whereas *Fer2* overexpression prevents, H_2O_2-induced PAM neuron loss. n=7-10 brains per group. Mann-Whitney test, **p<0.01, ***p<0.001, ****p<0.0001. **(b)** ROS levels in w^{1118} flies at different ages were monitored using H2DCF dye. Scale bar, 25 μm. **(c)** Quantification of ROS levels in the central brain from (**b**). Data are represented as mean ± SEM of the fold change relative to day 1. n=7-10 brains per group. One-way ANOVA followed by a Turkey's test for multiple group comparison, **p<0.01. **(d)** Brains of *Fer2::GFP::V5* flies of different ages were stained with anti-GFP (green) and PAM neurons were detected by anti-TH antibodies (magenta). Scale bar, 5 μm. **(e)** GFP and TH fluorescence intensities in the PAM region from (**d**) were quantified. Data are represented as mean ± SEM of the fold change relative to day 1. n=7-10 brains per group. One-way ANOVA followed by a Turkey's test for multiple group comparison, *p<0.05, ****p<0.0001.

Figure 3. Identification of *Fer2* transcriptional targets through a combination of ChIP-seq and RNA-seq approaches.

(a) ChIP-seq was performed on 14-day-old *Fer2::GFP::V5*, $Fer2^{1}$ flies. w^{1118} flies were used as a negative control. Two biological replicates per group. **(b)** A sequence containing an E-box (CANNTG, underlined) was found enriched in FER2 ChIP-seq peaks over w^{1118} ChIP-seq. **(c)** Scheme of the whole-head RNA-seq analysis to identify DEG after heat shock-driven *Fer2* transient overexpression. Three biological replicates per group. The number of DEGs

up- and downregulated after heat shock are shown**. (d)** Examples of ChIP-seq and RNA-seq data (48 h) for two *Fer2* direct targets, *CG8128* and *skd*. The rectangles indicate ChIP-seq peaks.

Figure 4. *Fer2* targets contribute to PAM neurons maintenance and mitochondrial health.

(a) Scheme of RNA-seq analysis of isolated PAM neurons to identify genes regulated by *Fer2* constitutive overexpression. Three biological replicates per group. **(b)** Intersection between peak-associated genes identified by FER2 ChIP-seq, DEG identified by whole-head RNA-seq 48 h after heat shock, and genes expressed in PAM neuron RNA-seq. **(c)** Network visualization of the 26 *Fer2* direct targets expressed in PAM neurons and their interactions. Each node represents a gene and is colored based on its function. The shape of the node indicates whether the gene is up- or downregulated by *Fer2*. The line thickness indicates the strength of data support. **(d)** Position of FER2 peaks and effect of *Fer2* overexpression on the expression of *Fer2* direct targets. **(e)** Volcano plot of 48 h heat shock RNA-seq data. Orange (downregulated) and blue (upregulated) dots indicate the 26 *Fer2* direct targets. **(f)** Functional validation of *Fer2* direct targets regarding their effect on PAM neuron survival. Quantification of the number of PAM neurons per hemisphere detected by anti-TH immunostaining in 35-day-old flies, upon overexpression (OE) or knock-down (RNAi) of the indicated gene in PAM neurons. n=7-10 per genotype. Genes that cause a statistically significant loss of PAM neurons are highlighted in red. A second independent replicate was assessed for these genes to confirm the significant loss of PAM neurons. One-way ANOVA followed by a Dunnett's test for multiple group comparison,**$p<0.01$, ****$p<0.0001$. **(g)** Network visualization of the most enriched GO terms among DEGs in PAM RNA-seq. GO terms were grouped into clusters based on their membership similarities. Each node

represents a GO term and is colored based on its cluster ID. GO terms that did not cluster are not shown. **(h)** Quantification of the number of PAM neurons per hemisphere, as detected by anti-TH immunostaining for the indicated genotypes and ages. *Sod2* overexpression in PAM neurons partially rescued PAM neuron loss in *Fer2*^{2} mutants. n=7-10 per group. One-way ANOVA followed by a Turkey's test for multiple group comparison, *p<0.05, ****p<0.0001.

Figure 5. *Nato3* is expressed in the midbrain DA neurons in adult mice. (a) Screenshot from GTEx portal (gtexportal.org) indicating *NATO3* expression levels in human tissues measured by RNA-seq. **(b)** RT-qPCR analysis of *Nato3* mRNA expression levels in different brain regions of C57BL6 mice at 4 months. OB, olfactory bulbs. PFC, prefrontal cortex. vMB, ventral midbrain. dMB, dorsal midbrain. Data are represented as mean ± SEM of the fold change relative to the expression in the OB. n=3 animals per region. One-way ANOVA followed by a Turkey's test for multiple group comparison, vMB vs any region other than dMB ***p<0.001, dMB vs any other region than vMB and cerebellum **p<0.01, dMB vs cerebellum #p<0.05. **(c)** RT-qPCR analysis of *Nato3* mRNA expression levels in the ventral midbrain of C57BL6 mice at different ages. Data are represented as mean ± SEM of the fold change relative to the expression at 1 month. n=3-5 animals per group. No statistically significant difference between different ages by ANOVA. **(d)** Representative images of anti-NATO3 (green) and anti-TH (magenta) immunostaining in coronal sections of the ventral midbrain of 14-month-old mice. The region shown in each raw is illustrated by the scheme on the right. Scale bars indicate 200 µm (top panels) and 50 µm (central and bottom panels).

Figure 6. *Nato3* cKO in DA neurons leads to age-dependent impairment in locomotor coordination and activity.

(a) Strategy for conditional ablation of *Nato3* in differentiated DA neurons. **(b)** RT-qPCR

analysis of *Nato3* mRNA levels in ventral midbrains of 2-month-old *Nato3*^{floxed} (ctrl) and *Nato3*$^{DAT\text{-}Cre}$ (cKO) mice. Data are represented as mean ± SEM of the fold change relative to the expression in ctrl. n=4 mice per genotype. Mann-Whitney test, *p<0.05. **(c)** The motor coordination of control and *Nato3* cKO mice was assessed at different ages using the pole test. The time taken to orient downward at the top of the pole (T-turn; left) and the total time to turn and descend the pole (T-tot; right) are shown. n=7-11 mice per group. Data are represented as mean ± SEM. Mann-Whitney test comparing ctrl and cKO of the same age, *p<0.05, **p<0.01. **(d)** Locomotor activity assessed at different ages using the voluntary wheel running test. The time spent running on the wheel (left) and the total distance run (right) are shown. n=7-11 mice per group. Data are represented as mean ± SEM. Mann-Whitney test comparing ctrl and cKO of the same age, *p<0.05. **(e)** Representative TH immunostaining images of coronal ventral midbrain sections from 16- to 18-month-old control and *Nato3* cKO mice. Scale bar, 200µm. **(f)** Quantification of TH^{+} neurons in SN and VTA from (**e**). n=3 mice per genotype. Data are represented as mean ± SD of the fold change relative to control. No statistically significant difference between ctrl and cKO by Mann-Whitney test. **(g)** Representative TH immunostaining images of coronal striatal sections from 16- to 18-month-old control and *Nato3* cKO mice. Scale bar, 200µm. **(h)** Optical densitometry from TH immunostaining of the dorsal striatum in (**g**). n=4 mice per genotype. Data are represented as mean ± SD of the fold change relative to control. No statistically significant difference between ctrl and cKO by Mann-Whitney test.

Figure 7. *Nato3* is essential for mitochondrial integrity in the midbrain DA neurons. **(a)** Mitochondria were visualized by anti-COX4 immunostaining (magenta) in TH^{+} neurons (green) of SN in 16- to 18-month-old control and *Nato3* cKO mice. Scale bar, 10µm. **(b)** The circularity of COX4^{+} mitochondria particles in TH^{+} neurons from (**a**) was measured and its

distribution was plotted in a histogram. The histogram for the cKO mouse is significantly right-shifted compared with that of the control. Kolmogorov-Smirnov test, $p<0.0001$. More than 700 $COX4^+$ particles per genotype were analyzed from three brains per genotype. **(c)** Electron micrographs of mitochondria from TH-labeled DA neurons from the SN of 16- to 18-month-old ctrl and *Nato3* cKO mice. The right bottom panel illustrates the difference between a degenerating mitochondrion in the dendrite of a *Nato3*-ablated TH^+ neuron, and a normal mitochondrion in an adjacent non-DA neuron. M, normal mitochondria. DM, degenerative mitochondria. Scale bar, 0.5 µm. **(d)** Classification criteria for mitochondria integrity (top) and mitochondria distribution in TH^+ neurons for ctrl and cKO mice (bottom). In total, 200 to 350 mitochondria from TH^+ neurons in SN were analyzed per genotype. **(e)** Measurement of size (left) and roundness (right) of mitochondria. 200 to 350 mitochondria from SN TH^+ neurons were analyzed per genotype. Data are represented as mean ± SEM. Mann-Whitney test, $**p<0.01$.

Supplementary Figure 1. *Fer2* loss of function and *Lrrk* gain of function or *park*^{1} mutation additively increase PAM neuron loss.

Quantification of the number of PAM neurons per hemisphere, as detected by anti-TH immunostaining for the indicated genotypes and ages. *Fer2>X* indicates that *UAS-transgene X* is expressed with *Fer2-GAL4*. n=7-10 brains per group. One-way ANOVA followed by a Turkey's test for multiple group comparison., $*p<0.05$, $**p<0.01$, $***p<0.001$, $****p<0.0001$. In (**a**), where brackets are not shown, flies overexpressing *Lrrk* and *Fer2-Gal4* flies (ctrl) of the same age are compared. In (**b**) at day 1**,** §$p<0.05$ when comparing *Fer2-Gal4, Fer2*^{2}/+ with *Fer2>Lrrk WT, Fer2*^{2}/+, and #$p<0.0001$ when comparing *Fer2-Gal4, Fer2*^{2}/+ with all the other genotypes. At day 14 and 35, &$p<0.0001$ when comparing *Fer2-Gal4, Fer2*^{2}/+ with all the other genotypes at the same age.

Supplementary Figure 2. ***Fer2::GFP::V5* transgene rescues PAM neuron loss and locomotor deficits in *Fer2*^{1} mutants.**

(a) Brains of *Fer2::GFP::V5, Fer2*^{1} flies at day 14 were stained with anti-GFP (green) and anti-TH (magenta) antibodies. The right panel presents a high-magnification image of the PAM neurons in the square from the left panel. Left panel scale bar, 50 µm. Right panel scale bar, 5 µm. **(b)** Quantification of the number of PAM neurons per hemisphere, as detected by anti-TH immunostaining in *w*^{1118}, *Fer2*^{1} and *Fer2::GFP::V5, Fer2*^{1} flies at day 14. n=7-10 brains per group. One-way ANOVA followed by a Turkey's test for multiple group comparison, ****p<0.0001. n.s., not significant. **(c)** Climbing index of *w*^{1118}, *Fer2*^{1} and *Fer2::GFP::V5, Fer2*^{1} flies at day 14. Data are represented as mean of three independent experiments ± SD. One-way ANOVA followed by a Turkey's test for multiple group comparison, ****p<0.0001. n.s., not significant.

Supplementary Fig. 3. Genetic pathways downstream of *Fer2*.

(a) List of transcription factors that are expressed in PAM neurons and whose binding sites are significantly overrepresented in the promoters of PAM RNA-seq DEGs. Enrichment p-value and the databases used for the analysis are indicated. Transcription factors known or predicted to interact with one or more *Fer2* direct targets are highlighted in orange. **(b)** Model of the role of *Fer2* in dopaminergic neuroprotection. *Fer2* binds to and regulates the expression of a set of direct target genes, including multiple transcription factors and chromatin regulators. *Fer2* direct targets FTZ-F1 and SMR interact with D, Br and USP and regulate a large set of genes within PAM neurons. In this manner, *Fer2* controls multiple pathways leading to regulation of mitochondrial gene expression, improved mitochondrial health, and PAM neuron survival against genetic and oxidative insults.

Supplementary Figure 4. Locomotor activity measured in the open field test is not affected in *Nato3* cKO mice.

Levels of horizontal activity (left), measured as the total distance traveled in the arena, and vertical activity (right), measured as the number of rearing events, were not different between *Nato3* cKO and control mice. n=5-7 mice per group. Data are represented as mean ± SEM. No statistically significant difference between ctrl and cKO by Mann-Whitney test.

1

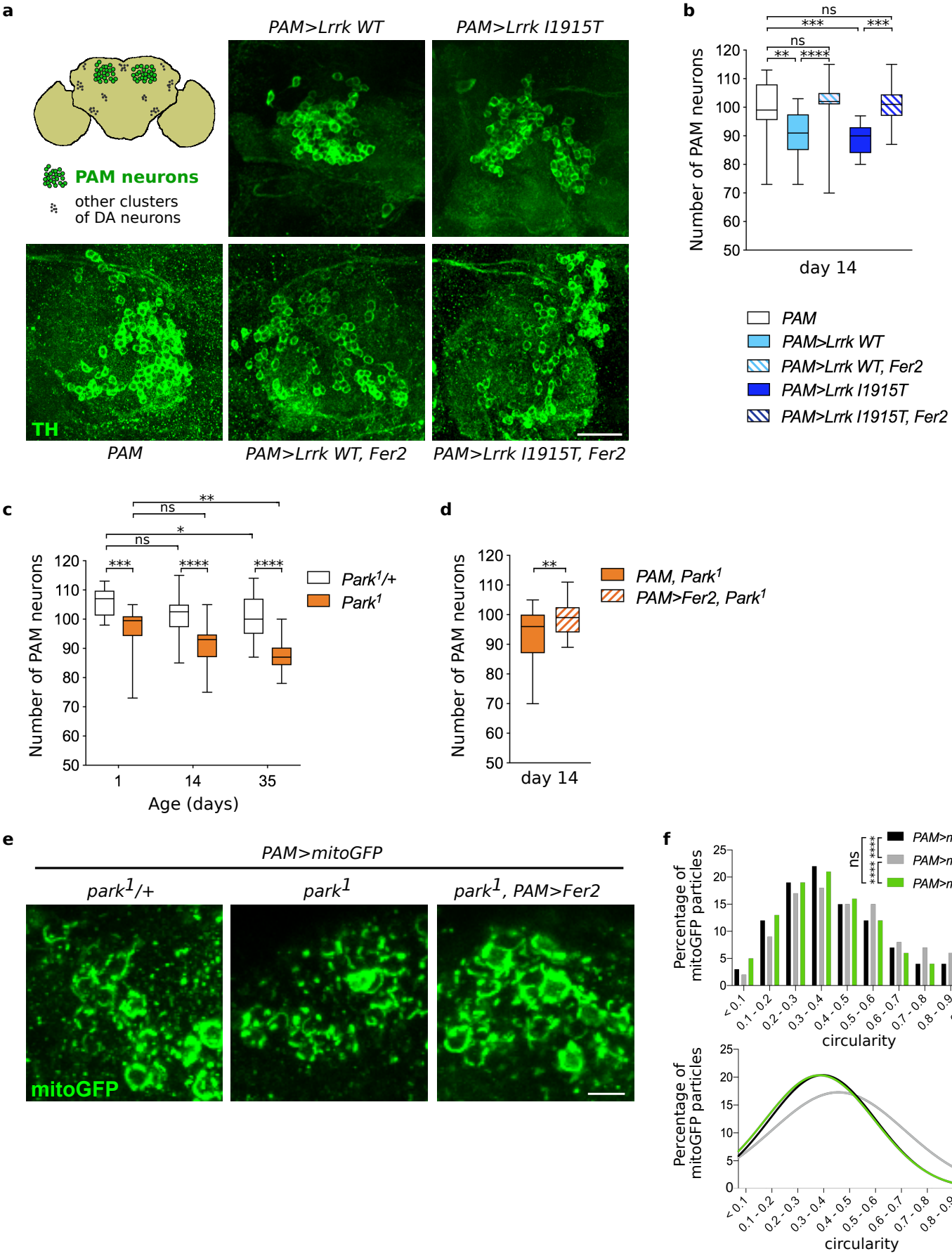
a
PAM>Lrrk WT
PAM>Lrrk I1915T
PAM neurons
other clusters of DA neurons
TH
PAM
PAM>Lrrk WT, Fer2
PAM>Lrrk I1915T, Fer2
b
Number of PAM neurons
day 14
ns
***
**
****
PAM
PAM>Lrrk WT
PAM>Lrrk WT, Fer2
PAM>Lrrk I1915T
PAM>Lrrk I1915T, Fer2
c
Number of PAM neurons
Age (days)
Park1/+
Park1
d
Number of PAM neurons
day 14
PAM, Park1
PAM>Fer2, Park1
e
PAM>mitoGFP
park1/+
park1
park1, PAM>Fer2
mitoGFP
f
Percentage of mitoGFP particles
circularity
PAM>mitoGFP, park1/+
PAM>mitoGFP, park1
PAM>mitoGFP, Fer2, park1

2

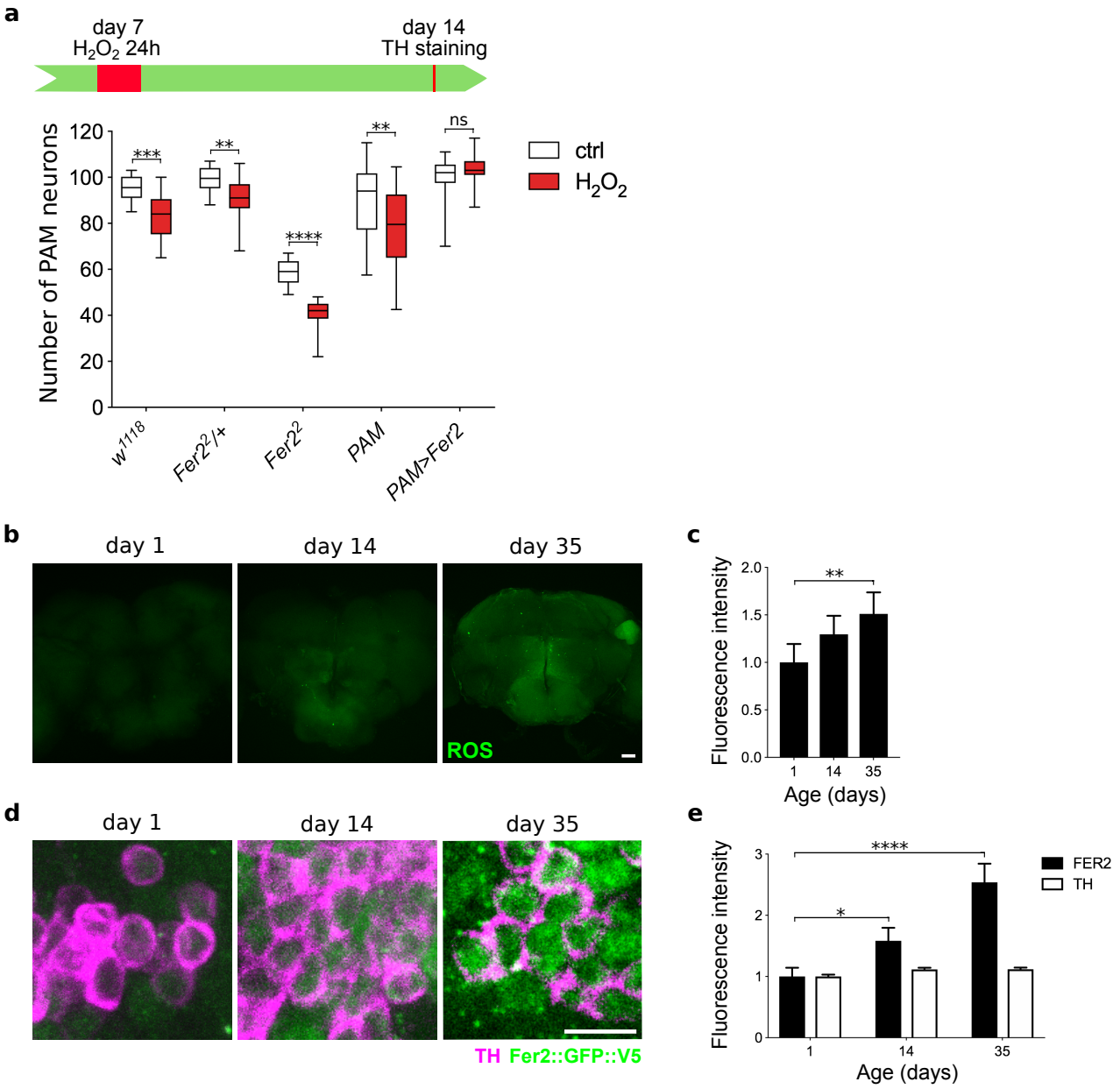
a
day 7
H_2O_2 24h
day 14
TH staining
Number of PAM neurons
120
100
80
60
40
20
0
***
**
****
**
ns
ctrl
H_2O_2
w^{1118}
$Fer2^2/+$
$Fer2^2$
PAM
PAM>Fer2
b
day 1
day 14
day 35
ROS
c
Fluorescence intensity
2.0
1.5
1.0
0.5
0.0
**
1
14
35
Age (days)
d
day 1
day 14
day 35
TH Fer2::GFP::V5
e
Fluorescence intensity
3
2
1
0
****
*
FER2
TH
1
14
35
Age (days)

3

a **ChIP-seq**

Fer2::GFP::V5, Fer2[1]

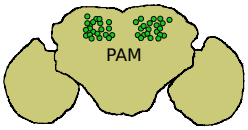

w[1118] (neg ctrl)

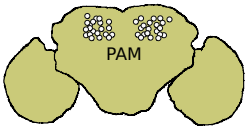

267 peaks
279 associated genes

b

p-value : e^{-42}

c **Head RNA-seq**

hs>Fer2
hs>Fer2 + heat-shock } DEG after heat-shock induced Fer2 OE

hs-Gal4
hs-Gal4 + heat-shock } DEG after heat-shock (independent on Fer2)

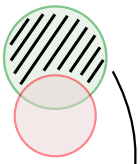

DEG after Fer2 OE (independent on heat-shock)

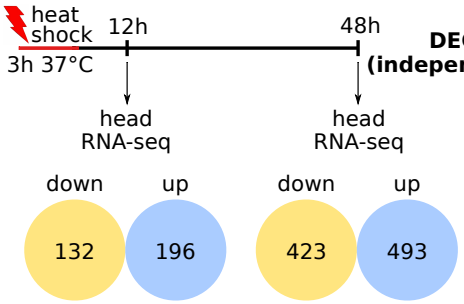

d

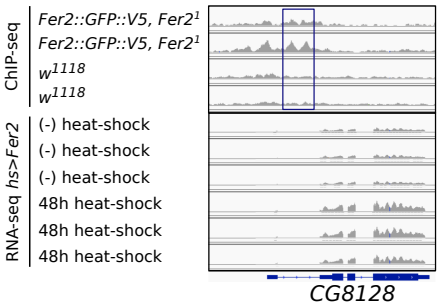

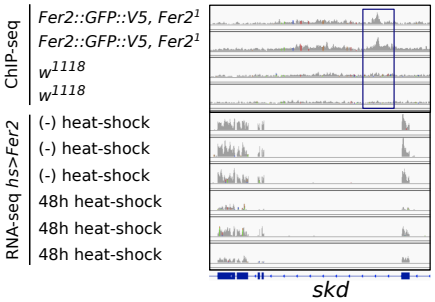

4

a

PAM RNA-seq

PAM>RedStinger ctrl

PAM>RedStinger, Fer2 OE

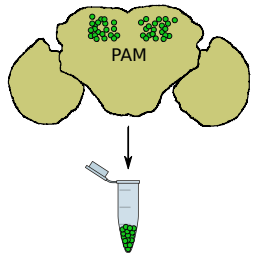

Brain dissociation and isolation of PAM neurons

PAM neuron transcriptome

7134 genes expressed in PAM
132 DEG, p-value<0.01

b

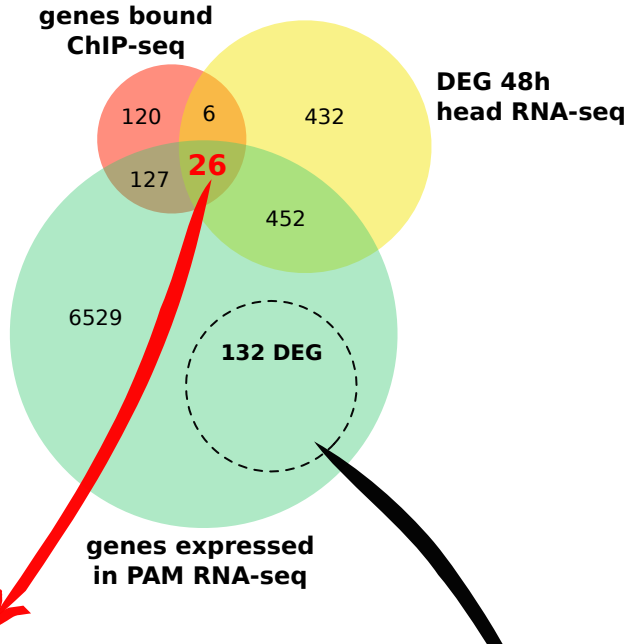

Fer2 direct targets

c

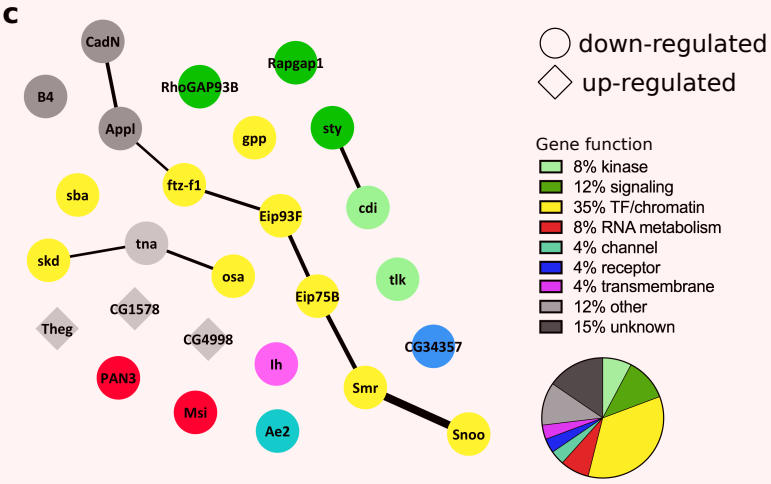

d

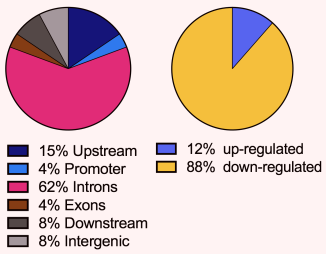

e

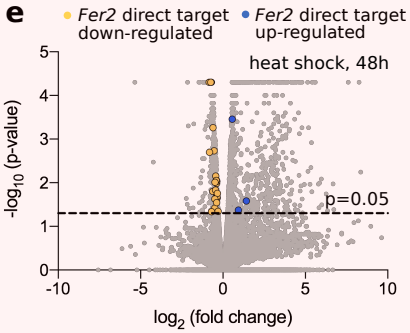

f

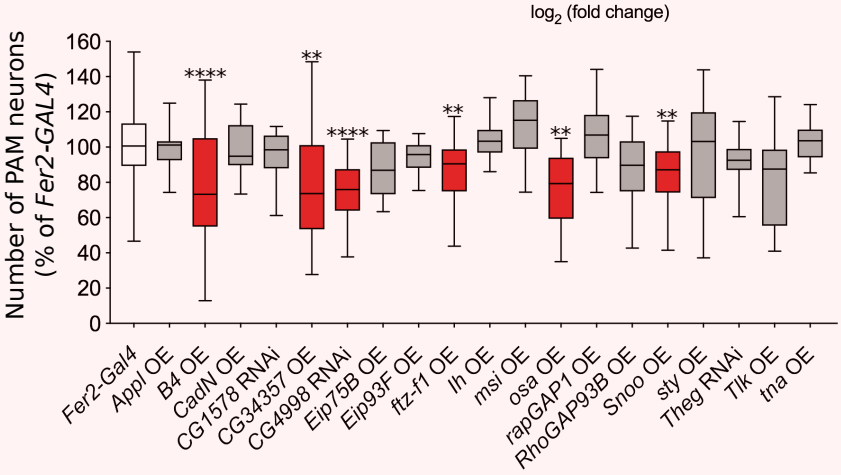

Fer2 secondary targets

g

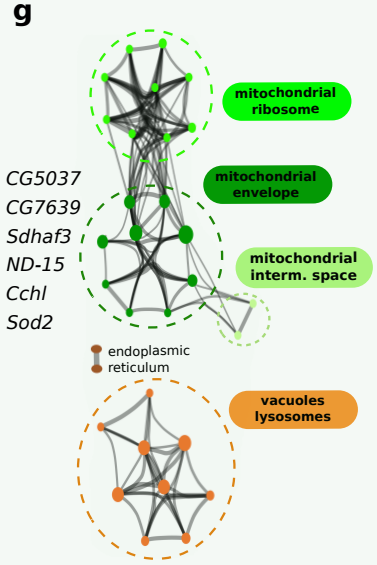

h

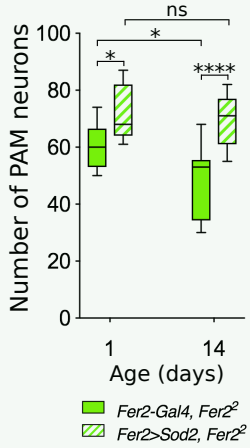

5

Human *NATO3* gene expression (gtexportal.org)

Mouse *Nato3* gene expression

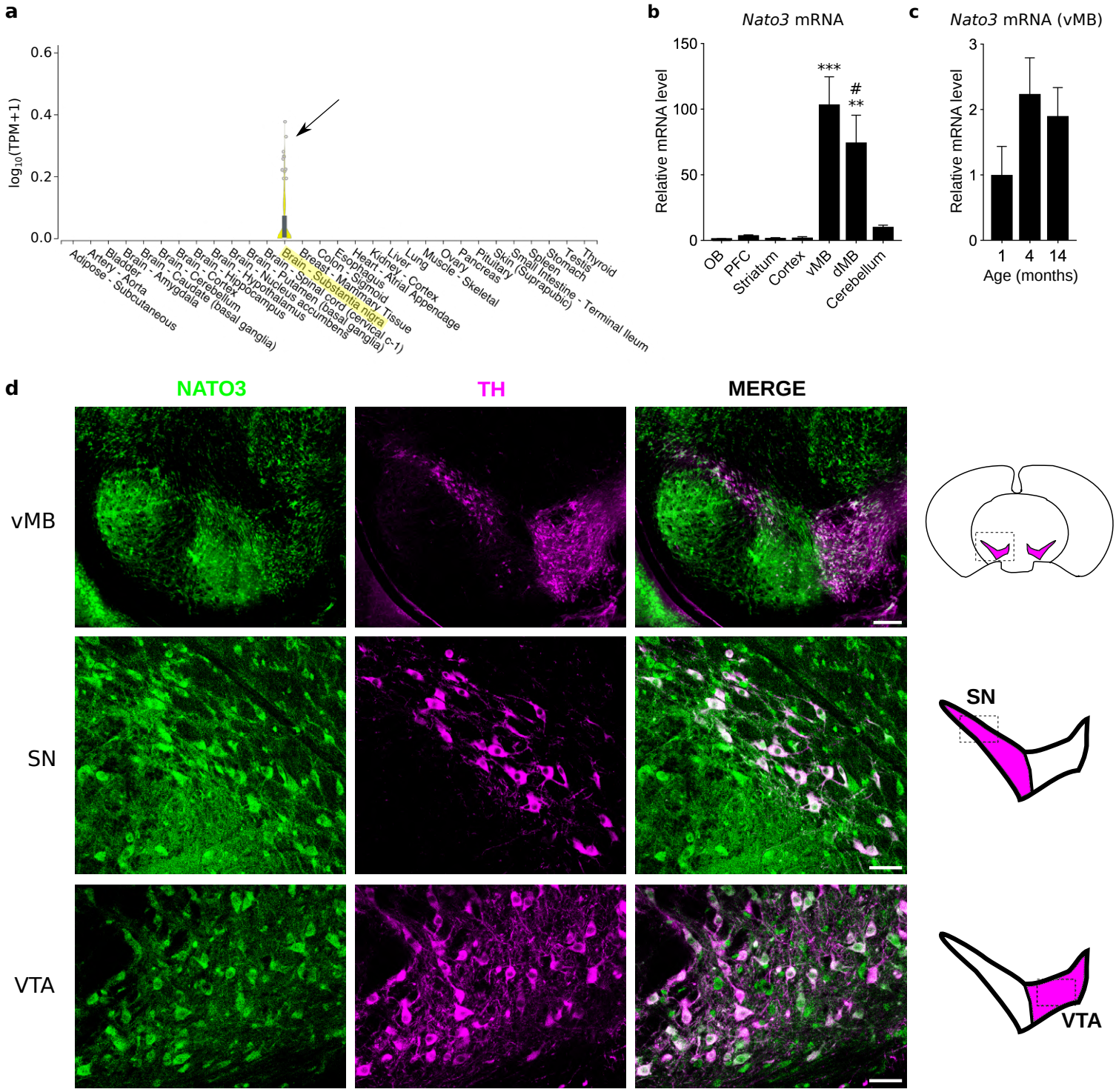

6

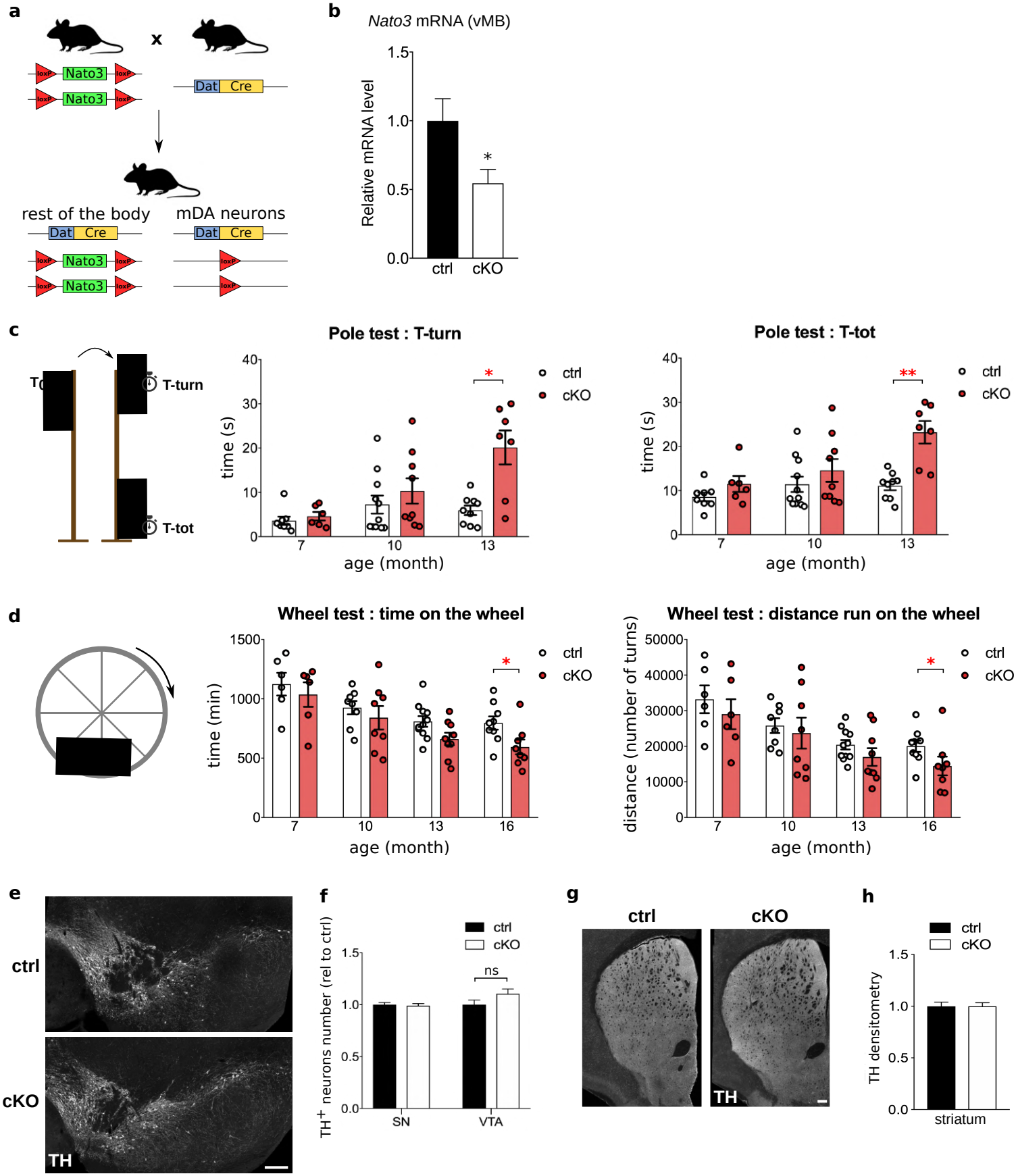
a
x
Nato3
Dat Cre
rest of the body
mDA neurons
b
Nato3 mRNA (vMB)
Relative mRNA level
ctrl
cKO
c
T-turn
T-tot
Pole test : T-turn
Pole test : T-tot
time (s)
age (month)
ctrl
cKO
d
Wheel test : time on the wheel
Wheel test : distance run on the wheel
time (min)
distance (number of turns)
e
ctrl
cKO
TH
f
TH+ neurons number (rel to ctrl)
ns
SN
VTA
g
ctrl
cKO
TH
h
TH densitometry
striatum

7

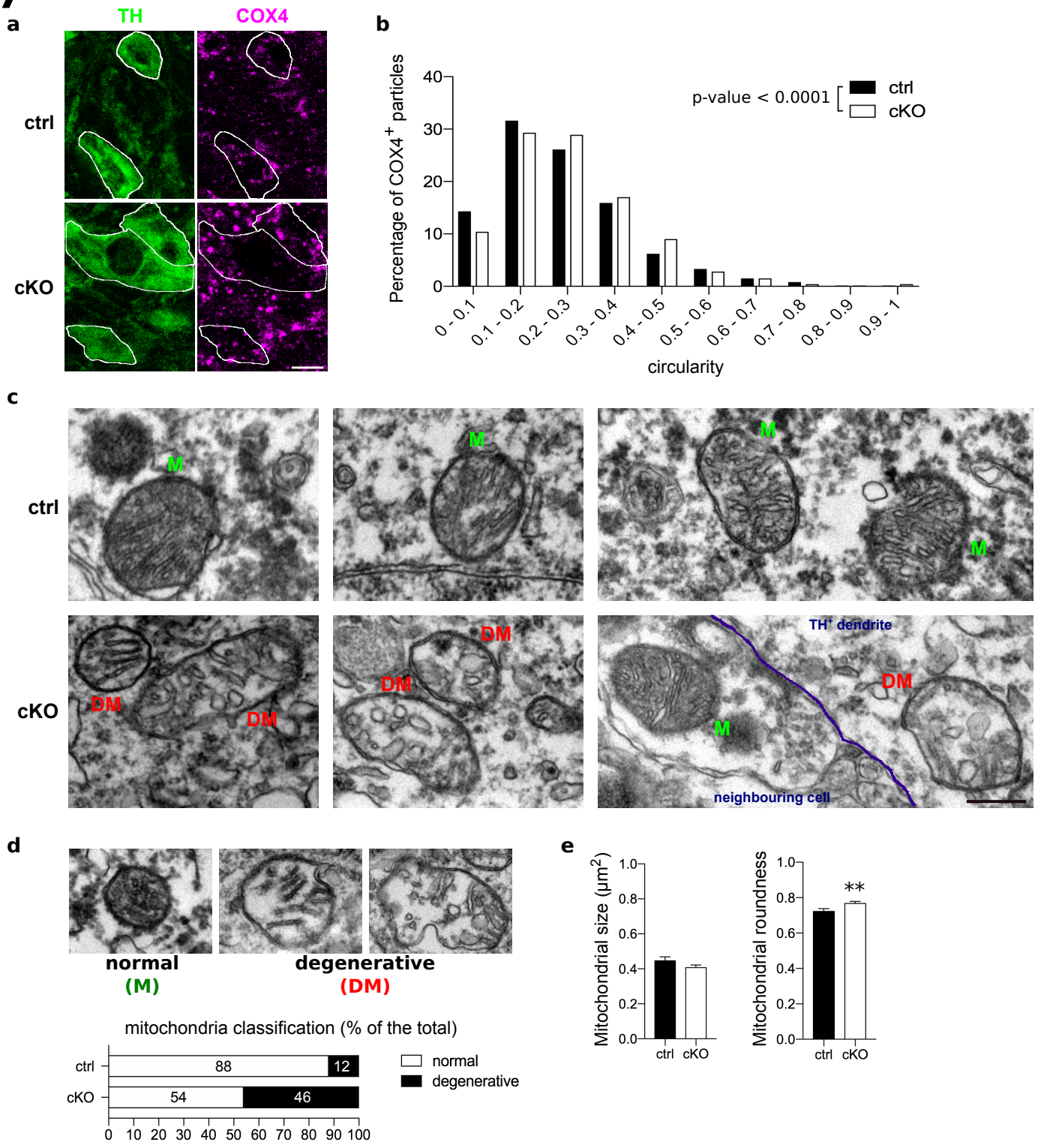
a
TH
COX4
ctrl
cKO
b
Percentage of COX4+ particles
p-value < 0.0001
ctrl
cKO
circularity
0 - 0.1
0.1 - 0.2
0.2 - 0.3
0.3 - 0.4
0.4 - 0.5
0.5 - 0.6
0.6 - 0.7
0.7 - 0.8
0.8 - 0.9
0.9 - 1
c
ctrl
cKO
M
DM
TH+ dendrite
neighbouring cell
d
normal
(M)
degenerative
(DM)
mitochondria classification (% of the total)
ctrl
cKO
88
12
54
46
normal
degenerative
e
Mitochondrial size (µm2)
Mitochondrial roundness
**